

https://dspace.org/

Thermodynamic activity of MnO in manganese slags and slag-metal equilibria

Cengizler, Hakan

2015-02-09
http://hdl.handle.net/10539/16928

Downloaded from a DSpace repository. https://dspace.org/

THERMODYNAMIC ACTIVITY OF MnO IN MANGANESE SLAGS AND SLAG-METAL EQUILIBRIA

Hakan Cengizler

A thesis submitted to the faculty of Engineering, University of the Witwatersrand, Johannesburg, in fulfilment of the requirements for the degree of Doctor of Philosophy.

Johannesburg, 1993

DECLARATION

I declare that this thesis is my own, unaided work. It is being submitted for the Degree of Doctor of Philosophy in the University of the Witwatersrand, Johannesburg. It has not been submitted before for any degree or examination in any other University.

(Signature of candidate)

5 day of October 1993

ACHIEVEMENTS

A fundamental study was conducted to measure the thermodynamic activity of manganese oxide in synthetic $MnO-CaO-MgO-SiO_2-Al_2O_3$ slags that are typically encountered in ferromanganese and silicomanganese production. Gas equilibration technique was used to determine the MnO activities in slags. A multi-coefficient regression model was developed to predict the activities of MnO in slags at 1500°C. The results were also fit into an existing slag model. Activities of Mn in Pt-Mn alloys at 1300°, 1400° and 1500°C were also re-determined. Slag-metal equilibrium experiments were conducted at 1500°C under a CO atmosphere to study the equilibrium distributions of important elements. It is believed that this work significantly contributes to the understanding of the behaviour of liquid slag and metal phases. It is also believed that the activity data gathered in this study can be used whenever necessary for new process developments, in conjunction with liquidus temperature, electrical conductivity and viscosity data that were measured earlier.

ABSTRACT

The aim of this study was to measure the thermodynamic activity of MnO in $MnO-CaO-MgO-SiO_2-Al_2O_3$ slags that are typically encountered in ferromanganese and silicomanganese production, and to establish equilibrium partition of various elements between ferromanganese alloy and the slag phase.

Gas equilibration technique was used to determine the MnO activities in slags which necessitated the re-determination of activities of Mn in Pt-Mn alloys at 1300°, 1400° and 1500°C which confirmed earlier results of strong negative deviations. MnO activities were determined by equilibrating slags of various compositions with Pt-Mn alloys under controlled partial pressure of oxygen in MnO saturated platinum crucibles at 1500°C. Activities of MnO were found to increase with increasing concentration of MnO, basicity and CaO-to-MgO ratio. A multi-coefficient regression model was developed to predict the activities of MnO in slags at 1500°C.

Slag-metal equilibrium experiments were conducted at 1500°C under a CO atmosphere utilizing graphite crucibles. The results have shown that the Mn distribution ratio increased with increasing concentration of silica in the slag and with decreasing basicity and CaO-to-Al_2O_3 ratio. The equilibrium carbon and manganese contents of the metal phase had linear relationship while carbon and silicon had inverse relationship. The carbon solubility in the metal phase increased with increasing Mn-to-Fe and Mn-to-Si ratios in the metal. While an increase in the basicity of the slag decreases the silicon content of the metal, it increases with increasing SiO_2 concentration of the slag. Multi-coefficient regression models were developed to predict the activity coefficient of manganese and silicon in the metal phase. The iso-activity contours of manganese and silicon were derived through the model equations in silicomanganese and ferromanganese compositions.

To the memory of my dear father,

Feyzi Cengizler

ACKNOWLEDGEMENTS

The author wishes to express his appreciation and thanks to:

Prof. R.Hurman Eric for advice, assistance and guidance throughout the course of this study.

The Council for Mineral Technology (MINTEK) for its financial support for this work of the Pyrometallurgy Research Group of the Metallurgy and Materials Engineering Department, University of the Witwatersrand.

The Ferroalloy Producers Association of South Africa (FAPA) for grants which assisted both the author and the Pyrometallurgy Research Group.

The Analytical Chemistry Division of MINTEK for analyzing the Pt strips, slag and metal samples.

CONTENTS **Page**

DECLARATION		ii
ABSTRACT		iv
DEDICATION		vi
ACKNOWLEDGEMENTS		vii
CONTENTS		viii
LIST OF FIGURES		xi
LIST OF TABLES		xxxi
1.	**INTRODUCTION**	**1**
1.1	History and uses of manganese and ferromanganese alloy	1
1.2	Manganese ore in the world and in South Africa	4
1.3	Production of carbon bearing ferromanganese	7
1.3.1	Production methods	7
1.3.2	Manganese oxide and their reduction reactions	8
1.4	The motivation of the present study	13
2.	**LITERATURE SURVEY**	**17**
2.1	General considerations	17
2.2	Pt-Mn binary system	20

2.3	Structure and properties of slags	25
2.3.1	Structure of silicate melts	29
2.3.2	Physical properties of slags	40
2.3.3	Thermodynamic properties of slags involving MnO	47
2.3.4	Slag Models	71
2.4	Thermodynamic properties of liquid manganese alloys	80
3	**EXPERIMENTAL TECHNIQUE AND PROCEDURE**	**96**
3.1	Experimental technique	96
3.1.1	Methods available for the measurements of activity of MnO in ferromanganese slags	96
3.1.2	Method adopted for the measurement of MnO activity in ferromanganese slags	101
3.2	Experimental set-up	104
3.2.1	The furnace assembly	104
3.2.2	The gas mixing system	108
3.2.3	Temperature control	110
3.3	Sample preparation	111
3.3.1	Platinum strips and crucibles	111
3.3.2	Preparation of synthetic $MnO-CaO-MgO-SiO_2-Al_2O_3$ slags	112
3.3.3	Preparation of Mn-Si-Fe-C alloys	115
3.4	Preliminary experiments and equilibration time	116

3.5	The procedure of Mn and MnO activity measurements	120
3.6	The procedure of slag-metal equilibrium experiments	121
3.7	Chemical analysis	123
4.	**RESULTS AND DISCUSSIONS**	**125**
4.1	Results of activity measurements	126
4.1.1	Activity-composition relations in Pt-Mn system	126
4.1.2	Activity of MnO in $CaO-MgO-SiO_2-Al_2O_3-MnO$ slags and modelling of results	134
4.1.2.1	Description of the slag model applied to the liquid mixture of an arbitrary number of oxides	149
4.1.2.2	Discussion of activity of MnO in ferromanganese slags	166
4.1.3	Activity coefficient of MnO in $CaO-MgO-SiO_2-Al_2O_3-MnO$ slags	189
4.2	The results of slag-metal equilibrium experiments	207
4.2.1	Manganese distribution	207
4.2.2	Silicon distribution	219
4.2.3	Manganese and silicon activities in Mn-Si-Fe-C melts	232
5.	**SUMMARY AND CONCLUSIONS**	**265**

6. APPENDICES **275**

APPENDIX A 275
APPENDIX A.1 275
APPENDIX A.2 279
APPENDIX B 283
APPENDIX B.1 283
APPENDIX B.2 288
APPENDIX B.3 289
APPENDIX C 301
APPENDIX D 325
APPENDIX E 350
APPENDIX E.1 350
APPENDIX E.2 355
APPENDIX E.3 360

7. REFERENCES **361**

LIST OF FIGURES

Figure		Page
Figure 1.	The activity coefficient of solid manganese measured by Abraham et al.[10] in solid Mn-Pt alloys at 1500° and 1650°C. The top line shows on the same scale, values for the activity coefficient of liquid iron in solid Fe-Pt alloys at 1550°C as measured by Larson and Chipman.	23
Figure 2.	Equilibrium concentration of Mn in Pt-Mn alloys[11].	23
Figure 3.	The variation with temperature and oxygen pressure of the Mn content of Pt-Mn alloys equilibrated with solid MnO[12].	26
Figure 4.	The variation with temperature and composition of $\ln\gamma_{Mn}$ in Pt-Mn alloys[12].	26
Figure 5.	The variation of $\ln\gamma_{Mn}$ with composition in Pt-Mn alloys studied in three previous studies[10,11,12].	27

Figure 6.	Relation between wave number of infrared absorption peak and SiO_2 content in binary silicate glasses[26].	35
Figure 7.	Diagram of Si-O tetrahedra in crystalline and molten silica.	39
Figure 8.	Diagram of dissolution of silica network by metal oxide.	39
Figure 9.	Activities of MnO in MnO-CaO-SiO_2 melts measured at 1500°C by Abraham, Davies and Richardson[52], dashed lines show the probable liquidus temperature in the system.	49
Figure 10.	Activities of MnO in MnO-CaO-SiO_2 melts measured at 1650°C by Abraham, Davies and Richardson[52], dashed lines show the probable liquidus temperature in the system.	49
Figure 11.	Activities of MnO in MnO-CaO-SiO_2 melts measured at 1650°C by Mehta and Richardson[53], dashed lines show the probable liquidus temperature in the system.	51
Figure 12.	Activities of MnO in MnO-MgO-SiO_2 melts measured at 1650°C by Mehta and Richardson[53], crosses show liquidus limits in binaries.	51

Figure 13.	Activities of MnO in MnO-BaO-SiO_2 melts measured at 1650°C by Mehta and Richardson[53], crosses show liquidus limits in binaries.	52
Figure 14.	Activities of MnO in MnO-CaO-Al_2O_3 melts measured at 1650°C by Mehta and Richardson[53], the limiting activities in MnO-Al_2O_3 are taken from Sharma and Richardson[51], crosses show liquidus limits in binaries.	52
Figure 15.	MnO and Al_2O_3 activities in MnO-Al_2O_3 melts measured at 1650°C by Sharma and Richardson[54]. Full lines and points represent results relative to solid MnO and Al_2O_3; heavy broken line relative to liquid MnO. Lightly broken lines show corresponding values for MnO and SiO_2 activities in MnO-SiO_2 melts at 1650°C taken from Abraham, Davies and Richardson[52].	53
Figure 16.	Activities of MnO measured at 1650°C by Sharma and Richardson[54] in MnO-SiO_2-Al_2O_3 melts relative to pure solid.	54
Figure 17.	Iso-activity coefficient curves of MnO, calculated by Turkdogan[57] and drawn for CaO-Al_2O_3-SiO_2 pseudo-ternary system for the	58

temperature range 1400°-1600°C; the liquidus isothermal drawn is for 1500°C.

Figure 18. The activity of MnO in MnO-SiO_2 melts at 1500°C determined by Rao and Gaskell[60], Abraham, Davies and Richardson[52] and Mehta and Richardson[53]. 63

Figure 19. The activity of SiO_2 in MnO-SiO_2 melts at 1500°C determined by Rao and Gaskell[60], Abraham, Davies and Richardson[52] and Mehta and Richardson[53]. 63

Figure 20. Ionic distributions for FeO-SiO_2 and CaO-SiO_2 melts at 1600°C calculated from Massons's[82] linear chain model. 78

Figure 21. Ionic distributions for FeO-SiO_2 melts in the temperature range 1257°-1407°C calculated from the branched chain model developed by Whiteway, Smith and Masson[83]. 78

Figure 22. Solubility of carbon in Fe-Mn-Si alloys at 1460°C after Petrushevskii and Gel'd[95] on the assumption that Fe%+Mn%+Si%=100, the different points correspond to variations of carbon content from 0.10 to 7.5 mass per cent. 82

Figure 23.	Solubility of carbon in the system Mn-Fe-Si-C at 1460°C after Burylev[101], Fe-to-Mn ratio equal to: 0 (system Mn-Si-C); 0.2; 0.4; 1.0; 3.0; and (system Fe-Si-C). Solid lines are calculated results.	84
Figure 24.	Solubility of graphite in Fe-Mn alloys reproduced from Skiredj and Elliot[103] using the data of Chipman et al.	84
Figure 25.	Solubility of graphite in Fe-Si alloys reproduced from Skiredj and Elliot[103] using the data of Chipman et al.	85
Figure 26.	Solubility of graphite in Fe-Mn-Si alloys at 1400°C reproduced from Skiredj and Elliot[103] using the data of Turkdogan and Hancock and *Herty and Royer.	86
Figure 27.	Solubility of graphite in Fe-Mn-Si alloys at 1550°C reproduced from Skiredj and Elliot[103] using the data of *Herty and Royer.	86
Figure 28.	Solubility of graphite in Fe-Mn-Si alloys at (x1600°C from Skiredj, from *Herty and Royer)[103].	87

Figure 29.	Solubility of graphite in Fe-Mn-Si alloys at 1650°C (*from Skiredj, *from Herty and Royer)[103].	87
Figure 30 a.	Isoactivity curves of Mn in the Mn-Fe-Si-C melts saturated with C at 1400°C[117].	92
Figure 30 b.	Isoactivity curves of Si in the Mn-Fe-Si-C melts saturated with C at 1500°C[119] ($\times 10^{-3}$). ▲, ■, ● and indicate the results in equilibrium with $MnO-SiO_2$, $CaO-MnO-SiO_2$, $CaO-MnO-Al_2O_3-SiO_2$ and $CaO-MnO-Al_2O_3-MgO-SiO_2$ slags respectively.	94
Figure 30 c.	Values of a^2_{MnO}/a_{SiO_2} in the $CaO-MnO-Al_2O_3-MgO-SiO_2$ slags equilibrated with Mn-Fe-Si-C melts saturated with C ($\times 10^{-3}$). Contour lines are drawn by using the values at 1600°C[119].	94
Figure 31.	A cross-section of the vertical molybdenum wound resistance furnace.	105
Figure 32.	The complete experimental set-up.	106
Figure 33.	Gas mixing apparatus.	109

Figure 34.	The change of activity coefficient of Mn with composition in Pt-Mn binary alloys at 1300°C.	127
Figure 35.	The change of activity coefficient of Mn with composition in Pt-Mn binary alloys at 1400°C.	129
Figure 36.	The change of activity coefficient of Mn with composition in Pt-Mn binary alloys at 1500°C.	130
Figure 37.	Activities of MnO in $MnO-CaO-MgO-SiO_2-Al_2O_3$ slags at 1500°C, B=0.58±0.02, CaO:MgO=∞, % Al_2O_3=5, optical basicity=0.68.	172
Figure 38.	Activities of MnO in $MnO-CaO-MgO-SiO_2-Al_2O_3$ slags at 1500°C, B=1.17±0.05, CaO:MgO=0.26±0.04, % Al_2O_3=5, optical basicity=0.66.	173
Figure 39.	Activities of MnO in $MnO-CaO-MgO-SiO_2-Al_2O_3$ slags at 1500°C, B=1.11±0.06, CaO:MgO=2.02±0.04, % Al_2O_3=5, optical basicity=0.70.	174
Figure 40.	Activities of MnO in $MnO-CaO-MgO-SiO_2-Al_2O_3$ slags at 1500°C, B=1.07±0.05, CaO:MgO=4.50±0.06, % Al_2O_3=5, optical basicity=0.73.	175

Figure 41. Activities of MnO in $MnO-CaO-MgO-SiO_2-Al_2O_3$ slags at 1500°C, B=0.83±0.04, CaO:MgO=3.65±0.06, % Al_2O_3=5, optical basicity=0.67. 176

Figure 42. Activities of MnO in $MnO-CaO-MgO-SiO_2-Al_2O_3$ slags at 1500°C, B=0.64±0.05, CaO:MgO=3.57±0.06, % Al_2O_3=5, optical basicity=0.65. 177

Figure 43. Activities of MnO in $MnO-CaO-MgO-SiO_2-Al_2O_3$ slags at 1500°C for various CaO-to-MgO ratios with B=0.40. 180

Figure 44. Activities of MnO in $MnO-CaO-MgO-SiO_2-Al_2O_3$ slags at 1500°C for various CaO-to-MgO ratios with B=0.60. 181

Figure 45. Activities of MnO in $MnO-CaO-MgO-SiO_2-Al_2O_3$ slags at 1500°C for various CaO-to-MgO ratios with B=0.80. 182

Figure 46. Activities of MnO in $MnO-CaO-MgO-SiO_2-Al_2O_3$ slags at 1500°C for various CaO-to-MgO ratios with B=1.00. 183

Figure 47.	Activities of MnO in $MnO-CaO-MgO-SiO_2-Al_2O_3$ slags at 1500°C for various basicity ratios with CaO:MgO=0.20.	185
Figure 48.	Activities of MnO in $MnO-CaO-MgO-SiO_2-Al_2O_3$ slags at 1500°C for various basicity ratios with CaO:MgO=2.00.	186
Figure 49.	Activities of MnO in $MnO-CaO-MgO-SiO_2-Al_2O_3$ slags at 1500°C for various basicity ratios with CaO:MgO=4.00.	187
Figure 50.	Activities of MnO in $MnO-CaO-MgO-SiO_2-Al_2O_3$ slags at 1500°C for various basicity ratios with CaO:MgO=6.00.	188
Figure 51.	The effect of different basicity ratios on the activities of MnO in $MnO-CaO-MgO-SiO_2-Al_2O_3$ slags at 1500°C with % MnO=15.	190
Figure 52.	The effect of different CaO-to-MgO ratios on the activities of MnO in $MnO-CaO-MgO-SiO_2-Al_2O_3$ slags at 1500°C with % MnO=15.	191
Figure 53.	The variation of MnO activity with composition in	192

$MnO-CaO-MgO-SiO_2-Al_2O_3$ slags at 1500°C, B=0.83±0.04, CaO:MgO=3.65±0.46, % Al_2O_3=5.

Figure 54. The variation of MnO activity with composition in $MnO-CaO-MgO-SiO_2-Al_2O_3$ slags at 1500°C, B=0.64±0.05, CaO:MgO=3.57±0.41, % Al_2O_3=5. 193

Figure 55. The variation of MnO activity with composition in $MnO-CaO-MgO-SiO_2-Al_2O_3$ slags at 1500°C, B=1.07±0.06, CaO:MgO=4.50±0.38, % Al_2O_3=5. 194

Figure 56. The variation of MnO activity with composition in $MnO-CaO-MgO-SiO_2-Al_2O_3$ slags at 1500°C, B=0.48±0.08, CaO:MgO=4.00±0.16, % Al_2O_3=5. 195

Figure 57. The variation of MnO activity with composition in $MnO-CaO-MgO-SiO_2-Al_2O_3$ slags at 1500°C, B=0.58±0.02, CaO:MgO=∞, % Al_2O_3=5. 196

Figure 58. The variation of MnO activity with composition in $MnO-CaO-MgO-SiO_2-Al_2O_3$ slags at 1500°C, B=0.90±0.07, CaO:MgO=2.06±0.19, % Al_2O_3=5. 197

Figure 59.	The variation of MnO activity with composition in $MnO-CaO-MgO-SiO_2-Al_2O_3$ slags at 1500°C, B=1.11±0.06, CaO:MgO=2.02±0.12, % Al_2O_3=5.	198
Figure 60.	The variation of activity coefficient of MnO with composition in $MnO-CaO-MgO-SiO_2-Al_2O_3$ slags at 1500°C, B=1.11±0.06, CaO:MgO=2.02±0.12, % Al_2O_3=5.	200
Figure 61.	The variation of activity coefficient of MnO with composition in $MnO-CaO-MgO-SiO_2-Al_2O_3$ slags at 1500°C, B=0.83±0.04, CaO:MgO=3.65±0.46, % Al_2O_3=5.	201
Figure 62.	The variation of activity coefficient of MnO with composition in $MnO-CaO-MgO-SiO_2-Al_2O_3$ slags at 1500°C, B=1.07±0.06, CaO:MgO=4.50±0.38, % Al_2O_3=5.	202
Figure 63.	The variation of activity coefficient of MnO with composition in $MnO-CaO-MgO-SiO_2-Al_2O_3$ slags at 1500°C, B=0.58±0.02, CaO:MgO=∞, % Al_2O_3=5.	203
Figure 64.	The variation of activity coefficient of MnO with composition	204

in $MnO-CaO-MgO-SiO_2-Al_2O_3$ slags at 1500°C, B=1.15±0.03, $CaO:MgO$=1.59±0.11, % Al_2O_3=5.

Figure 65. The variation of activity coefficient of MnO with composition in $MnO-CaO-MgO-SiO_2-Al_2O_3$ slags at 1500°C, B=0.43±0.02, $CaO:MgO$=3.79±0.37, % Al_2O_3=5. 205

Figure 66. The effect of basicity ratio on the manganese distribution at 1500°C under CO atmosphere. 212

Figure 67. The effect of the SiO_2 content of the slag on manganese distribution with Si:Fe=0.23 in the metal phase at 1500°C under CO atmosphere. 214

Figure 68. The effect of the SiO_2 content of the slag on manganese distribution with Si:Fe=0.18 in the metal phase at 1500°C under CO atmosphere. 215

Figure 69. The effect of the CaO-to-Al_2O_3 ratio of the slag on manganese distribution with Si:Fe=0.23 in the metal phase at 1500°C under CO atmosphere. 216

Figure 70. The effect of the MgO-to-CaO ratio of the slag on manganese 218

distribution with different MnO concentrations at 1500°C under CO atmosphere.

Figure 71. The effect of the Mn content on the C content of the metal phase with Si:Fe=0.18 at 1500°C under CO atmosphere. 220

Figure 72. The effect of the basicity on the Mn content of the slags at 1500°C under CO atmosphere. 221

Figure 73. The effect of the Si content on the C content of the metal phase with different Mn-to-Fe ratios at 1500°C under CO atmosphere. 223

Figure 74. The effect of the Si content on the C content of the metal phase with different Mn-to-Si ratios at 1500°C under CO atmosphere. 224

Figure 75. The effect of the SiO_2 content of the slag phase on the Si content of the metal phase with different Mn-to-Fe ratios at 1500°C under CO atmosphere. 226

Figure 76. The effect of the SiO_2 content of the slag phase on the Si content of the metal phase with different Mn-to-Si ratios at 1500°C under CO atmosphere. 227

Figure 77.	The effect of the CaO-to-Al_2O_3 ratio of the slag phase on the Si content of the metal phase with different Mn-to-Fe ratios at 1500°C under CO atmosphere.	228
Figure 78.	The effect of the CaO-to-Al_2O_3 ratio of the slag phase on the Si content of the metal phase with different Mn-to-Si ratios at 1500°C under CO atmosphere.	229
Figure 79.	The effect of the MgO-to-CaO ratio of the slag on the Si distribution with 5% Al_2O_3 and 53.1% SiO_2 at 1500°C under CO atmosphere.	231
Figure 80.	The effect of the basicity ratio of the slag on the Si content of the metal phase at 1500°C under CO atmosphere.	233
Figure 81.	Iso-activity lines of Si in silicomanganese melts saturated with C at 1500°C.	255
Figure 82.	Iso-activity lines of Si in ferromanganese melts saturated with C at 1500°C ($\times 10^{-4}$).	256
Figure 83.	Liquidus projection of Fe-Mn-C system[131].	258

Figure 84.	Iso-activity lines of Mn in silicomanganese melts saturated with C at 1500°C.	261
Figure 85.	Iso-activity lines of Si in silicomanganese melts saturated with C at 1500°C ($\times 10^{-3}$).	262
Figure A.1.	Flowrate of CO through capillary tube.	276
Figure A.2.	Flowrate of CO_2 through capillary tube.	277
Figure A.3.	p_{O_2} values that can be obtained by various CO_2-to-CO ratios at different temperatures.	280
Figure A.4.	Non-stoichiometry of MnO[15] as a function of oxygen pressure (between 1500°-1650°C). Broken line is theoretical curve.	281
Figure A.5.	Activity of stoichiometric MnO[15] in the non-stoichiometric oxide as a function of oxygen pressure.	282
Figure B.1.1.	Manganese picked up by platinum from pure MnO as a function of time at 1300°C.	283

Figure B.1.2. Manganese picked up by platinum from pure MnO as a function of time at 1400°C. 284

Figure B.1.3. Manganese picked up by platinum from pure MnO as a function of time at 1500°C. 285

Figure B.1.4. Manganese picked up by platinum from $MnO-CaO-MgO-SiO_2-Al_2O_3$ slag as a function of time at 1500°C. 286

Figure B.1.5. Equilibration time determination experiments for slag-metal equilibria between $MnO-CaO-MgO-SiO_2-Al_2O_3$ slags and Mn-Si-Fe-C metal phase at 1500°C. 287

Figure C.1. Activities of MnO in $MnO-CaO-MgO-SiO_2-Al_2O_3$ slags at 1500°C, B=0.65±0.03, CaO:MgO=3.18±0.04, % Al_2O_3=5, optical basicity=0.67. 301

Figure C.2. Activities of MnO in $MnO-CaO-MgO-SiO_2-Al_2O_3$ slags at 1500°C, B=1.08±0.02, CaO:MgO=3.44±0.07, % Al_2O_3=5, optical basicity=0.72. 302

Figure C.3. Activities of MnO in $MnO-CaO-MgO-SiO_2-Al_2O_3$ slags at 303

1500°C, B=0.69±0.05,
CaO:MgO=1.99±0.06, % Al_2O_3=5,
optical basicity=0.65.

Figure C.4. Activities of MnO in $MnO-CaO-MgO-SiO_2-Al_2O_3$ slags at 1500°C, B=0.43±0.01, CaO:MgO=2.38±0.04, % Al_2O_3=5, optical basicity=0.67. 304

Figure C.5. Activities of MnO in $MnO-CaO-MgO-SiO_2-Al_2O_3$ slags at 1500°C, B=0.61±0.03, CaO:MgO=5.05±0.04, % Al_2O_3=5, optical basicity=0.67. 305

Figure C.6. Activities of MnO in $MnO-CaO-MgO-SiO_2-Al_2O_3$ slags at 1500°C, B=0.88±0.01, CaO:MgO=2.90±0.05, % Al_2O_3=5, optical basicity=0.68. 306

Figure C.7. Activities of MnO in $MnO-CaO-MgO-SiO_2-Al_2O_3$ slags at 1500°C, B=0.43±0.02, CaO:MgO=3.79±0.06, % Al_2O_3=5, optical basicity=0.63. 307

Figure C.8. Activities of MnO in $MnO-CaO-MgO-SiO_2-Al_2O_3$ slags at 1500°C, B=1.02±0.05, CaO:MgO=2.86±0.07, % Al_2O_3=5, optical basicity=0.71. 308

Figure C.9. Activities of MnO in $MnO-CaO-MgO-SiO_2-Al_2O_3$ slags at 1500°C, B=0.91±0.04, CaO:MgO=1.47±0.05, % Al_2O_3=5, optical basicity=0.69. 309

Figure C.10. Activities of MnO in $MnO-CaO-MgO-SiO_2-Al_2O_3$ slags at 1500°C, B=0.48±0.05, CaO:MgO=4.00±0.05, % Al_2O_3=5, optical basicity=0.64. 310

Figure C.11. Activities of MnO in $MnO-CaO-MgO-SiO_2-Al_2O_3$ slags at 1500°C, B=0.78±0.02, CaO:MgO=∞, % Al_2O_3=5, optical basicity=0.70. 311

Figure C.12. Activities of MnO in $MnO-CaO-MgO-SiO_2-Al_2O_3$ slags at 1500°C, B=0.90±0.05, CaO:MgO=2.06±0.06, % Al_2O_3=5, optical basicity=0.68. 312

Figure C.13. Activities of MnO in $MnO-CaO-MgO-SiO_2-Al_2O_3$ slags at 1500°C, B=1.15±0.03, CaO:MgO=1.59±0.04, % Al_2O_3=5, optical basicity=0.69. 313

Figure C.14. Activities of MnO in $MnO-CaO-MgO-SiO_2-Al_2O_3$ slags at 1500°C, B=0.68±0.04, CaO:MgO=5.66±0.05, % Al_2O_3=5, optical basicity=0.66. 314

Figure C.15. Activities of MnO in $MnO-CaO-MgO-SiO_2-Al_2O_3$ slags at 1500°C, B=0.56±0.05, CaO:MgO=3.45±0.06, % Al_2O_3=5, optical basicity=0.66. 315

Figure C.16. Activities of MnO in $MnO-CaO-MgO-SiO_2-Al_2O_3$ slags at 1500°C for various CaO-to-MgO ratios with B=0.40. 316

Figure C.17. Activities of MnO in $MnO-CaO-MgO-SiO_2-Al_2O_3$ slags at 1500°C for various CaO-to-MgO ratios with B=0.60. 317

Figure C.18. Activities of MnO in $MnO-CaO-MgO-SiO_2-Al_2O_3$ slags at 1500°C for various CaO-to-MgO ratios with B=0.80. 318

Figure C.19. Activities of MnO in $MnO-CaO-MgO-SiO_2-Al_2O_3$ slags at 1500°C for various CaO-to-MgO ratios with B=1.00. 319

Figure C.20. Activities of MnO in $MnO-CaO-MgO-SiO_2-Al_2O_3$ slags at 1500°C for various CaO-to-MgO ratios with B=1.20. 320

Figure C.21. Activities of MnO in $MnO-CaO-MgO-SiO_2-Al_2O_3$ slags at 1500°C for various CaO-to-MgO ratios with B=1.20. 321

Figure C.22. Activities of MnO in $MnO-CaO-MgO-SiO_2-Al_2O_3$ slags at 1500°C for various basicity ratios with CaO:MgO=8.00. 322

Figure C.23. Activities of MnO in $MnO-CaO-MgO-SiO_2-Al_2O_3$ slags at 1500°C for various basicity ratios with CaO:MgO=10.00. 323

Figure C.24. Activities of MnO in $MnO-CaO-MgO-SiO_2-Al_2O_3$ slags at 1500°C for various basicity ratios with CaO:MgO=∞. 324

Figure D.1. The effect of the CaO-to-Al_2O_3 ratio of the slag on manganese distribution with Si:Fe=0.18 in the metal phase at 1500°C under CO atmosphere. 325

Figure D.2. The effect of the MgO-to-CaO ratio of the slag on the Mn distribution with 5% Al_2O_3 and 4.43% MnO at 1500°C under CO atmosphere. 326

Figure D.3.	The effect of the MgO-to-CaO ratio of the slag on the Mn-distribution with 5% Al_2O_3 and 9.53% MnO at 1500°C under CO atmosphere.	327
Figure D.4.	The effect of the MgO-to-CaO ratio of the slag on the Mn distribution with 5% Al_2O_3 and 10.57% MnO at 1500°C under CO atmosphere.	328
Figure D.5.	The effect of the MgO-to-CaO ratio of the slag on the Mn distribution with 5% Al_2O_3 and 11.42% MnO at 1500°C under CO atmosphere.	329
Figure D.6.	The effect of the Si content on the C content of the metal phase with Mn:Fe=7.4 at 1500°C under CO atmosphere.	330
Figure D.7.	The effect of the Si content on the C content of the metal phase with Mn:Fe=66.7 at 1500°C under CO atmosphere.	331
Figure D.8.	The effect of the Si content on the C content of the metal phase with Mn:Fe=3.7 at 1500°C under CO atmosphere.	332
Figure D.9.	The effect of the Si content on the C content of the metal phase with Mn:Si=2.9 at 1500°C under CO atmosphere.	333

Figure D.10. The effect of the Si content on the C content of the metal phase with Mn:Si=3.5 at 1500°C under CO atmosphere. 334

Figure D.11. The effect of the Si content on the C content of the metal phase with Mn:Si=4.5 at 1500°C under CO atmosphere. 335

Figure D.12. The effect of the Si content on the C content of the metal phase with Mn:Si=5.6 at 1500°C under CO atmosphere. 336

Figure D.13. The effect of the SiO_2 content of the slag phase on the Si content of the metal phase with Mn:Fe=3.7 at 1500°C under CO atmosphere. 337

Figure D.14. The effect of the SiO_2 content of the slag phase on the Si content of the metal phase with Mn:Fe=5.5 at 1500°C under CO atmosphere. 338

Figure D.15. The effect of the SiO_2 content of the slag phase on the Si content of the metal phase with Mn:Fe=6.7 at 1500°C under CO atmosphere. 339

Figure D.16. The effect of the SiO_2 content of the slag phase on the Si content of the metal phase with Mn:Si=2.9 at 1500°C under CO atmosphere. 340

Figure D.17. The effect of the SiO_2 content of the slag phase on the Si content of the metal phase with Mn:Si=3.5 at 1500°C under CO atmosphere. 341

Figure D.18. The effect of the SiO_2 content of the slag phase on the Si content of the metal phase with Mn:Si=4.5 at 1500°C under CO atmosphere. 342

Figure D.19. The effect of the SiO_2 content of the slag phase on the Si content of the metal phase with Mn:Si=5.6 at 1500°C under CO atmosphere. 343

Figure D.20. The effect of the CaO-to-Al_2O_3 ratio of the slag phase on the Si content of the metal phase with Mn:Fe=3.7 at 1500°C under CO atmosphere. 344

Figure D.21. The effect of the CaO-to-Al_2O_3 ratio of the slag phase on the Si content of the metal phase with Mn:Fe=7.4 at 1500°C under CO atmosphere. 345

Figure D.22. The effect of the CaO-to-Al_2O_3 ratio of the slag phase on the Si content of the metal phase with Mn:Si=2.9 at 1500°C under CO atmosphere. 346

Figure D.23. The effect of the CaO-to-Al_2O_3 ratio of the slag phase on the Si content of the metal phase with Mn:Si=3.5 at 1500°C under CO atmosphere. 347

Figure D.24. The effect of the CaO-to-Al_2O_3 ratio of the slag phase on the Si content of the metal phase with Mn:Si=4.5 at 1500°C under CO atmosphere. 348

Figure D.25. The effect of the CaO-to-Al_2O_3 ratio of the slag phase on the Si content of the metal phase with Mn:Si=5.6 at 1500°C under CO atmosphere. 349

LIST OF TABLES

Table		Page
Table I.	Compositions of different ferromanganese alloys[3].	4
Table II.	World production of manganese ore (in million short tons)[1].	6
Table III.	Estimate of reserves in the Kalahari manganese deposit[7].	7
Table IV.	The initial slag compositions.	114
Table V.	The initial metal-phase compositions.	116
Table VI.	The compositions, the activity and the activity coefficients of Mn in Pt-Mn binary alloys at 1300°C.	132
Table VII.	The compositions, the activity, and the activity coefficients of Mn in Pt-Mn binary alloys at 1400°C.	132
Table VIII.	The compositions, the activity, and the activity coefficients of Mn in Pt-Mn binary alloys at 1500°C.	133
Table IX.	Model parameters for activity coefficient of manganese.	133

Table X.	Activity of MnO in $CaO-MgO-SiO_2-Al_2O_3-MnO$ slags at 1500°C with pure liquid MnO as the standard state.	135
Table XI.	Results for MnO activity model.	145
Table XII.	Model parameters for MnO activities and coefficients for MnO activity models.	147
Table XIII.	Energy parameters used in the model[89].	153
Table XIV.	Nomenclature for the definition of the various symbols used in the expression of the thermodynamic functions of the liquid mixture of oxides[89].	154
Table XV.	Enthalpy and entropy of change of reference state for the various components[89].	161
Table XVI	Free energy of formation of stoichiometric compounds from pure components taken in the reference state of Table XV values used in the model[88].	164
Table XVII.	Optical basicity of various oxides[124].	171

Table XVIII.	Optical basicity values calculated from sulphide capacity data[124].	171
Table XIX.	The results of the equilibrium experiments in ferromanganese composition at 1500oC and CO atmosphere.	208
Table XX.	The results of the equilibrium experiments in silicomanganese composition at 1500oC and CO atmosphere.	210
Table XXI.	Activities of silicon and manganese in silicomanganese metal phase.	236
Table XXII.	Activities of silicon and manganese in ferromanganese metal phase.	238
Table XXIII.	Activity coefficients of silicon in silicomanganese metal phase.	240
Table XXIV.	Activity coefficients of silicon in ferromanganese metal phase.	242
Table XXV.	Results for $\ln\gamma_{Si}$ model in silicomanganese metal phase.	244
Table XXVI.	Results for $\ln\gamma_{Si}$ model in ferromanganese metal phase.	244
Table XXVII.	Model parameters for $\ln\gamma_{Si}$ and coefficients for $\ln\gamma_{Si}$ models.	245

Table XXVIII.	Activity coefficients of manganese in silicomanganese metal phase.	248
Table XXIX	Activity coefficients of manganese in ferromanganese metal phase.	250
Table XXX.	Results for $\ln\gamma_{Mn}$ model in silicomanganese metal phase.	252
Table XXXI.	Results for $\ln\gamma_{Mn}$ model in ferromanganese metal phase.	252
Table XXXII.	Model parameters for $\ln\gamma_{Mn}$ and coefficients for $\ln\gamma_{Mn}$ models.	253
Table B.3.1.	The SEM-EDAX analysis of Pt-Mn alloy sample by line scanning (Pt-Mn system, equilibration time is 48 hours at 1300°C and p_{O_2}=4.17x10^{-9} atm, Mn content determined by chemical analysis is 6.59 mass per cent).	290
Table B.3.2.	The SEM-EDAX analysis of Pt-Mn alloy sample by line scanning (Pt-Mn system, equilibration time is 48 hours at 1300°C and p_{O_2}=5.54x10^{-11} atm, Mn content determined by chemical analysis is 10.7 mass per cent).	291

Table B.3.3. The SEM-EDAX analysis of Pt-Mn alloy sample by line scanning (Pt-Mn system, equilibration time is 24 hours at 1400°C and p_{O_2}=6.78x10^{-8} atm, Mn content determined by chemical analysis is 6.05 mass per cent). 292

Table B.3.4. The SEM-EDAX analysis of Pt-Mn alloy sample by line scanning (Pt-Mn system, equilibration time is 24 hours at 1400°C and p_{O_2}=2.35x10^{-10} atm, Mn content determined by chemical analysis is 12.2 mass per cent). 293

Table B.3.5. The SEM-EDAX analysis of Pt-Mn alloy sample by line scanning (Pt-Mn system, equilibration time is 24 hours at 1500°C and p_{O_2}=9.30x10^{-8} atm, Mn content determined by chemical analysis is 10.5 mass per cent). 294

Table B.3.6. The SEM-EDAX analysis of Pt-Mn alloy sample by line scanning (Pt-Mn system, equilibration time is 24 hours at 1500°C and p_{O_2}=4.76x10^{-7} atm, Mn content determined by chemical analysis is 6.25 mass per cent). 295

Table B.3.7. The SEM-EDAX analysis of Pt-Mn alloy sample by line scanning (Pt-Mn system, equilibration time is 24 hours at 1500°C and p_{O_2}=4.99x10^{-11} atm, Mn content determined by chemical analysis is 19.5 mass per cent). 296

Table B.3.8. The SEM-EDAX analysis of Pt-Mn alloy sample by line scanning (Pt-Mn system, equilibration time is 24 hours at 1500°C and p_{O_2}=4.98x10^{-10} atm, Mn content determined by chemical analysis is 14.9 mass per cent). 297

Table B.3.9. The SEM-EDAX analysis of Pt-Mn alloy sample by line scanning (Pt-Mn system, equilibration time is 24 hours at 1500°C and p_{O_2}=5.19x10^{-6} atm, Mn content determined by chemical analysis is 3.57 mass per cent). 298

Table B.3.10. The SEM-EDAX analysis of Pt-Mn alloy sample by line scanning (MnO-CaO-MgO-SiO_2-Al_2O_3 system, equilibration time is 24 hours at 1500°C and p_{O_2}=5.80x10^{-8} atm, Mn content determined by chemical analysis is 3.22 mass per cent). 299

Table B.3.11. The SEM-EDAX analysis of Pt-Mn alloy sample by line scanning ($MnO-CaO-MgO-SiO_2-Al_2O_3$ system, equilibration time is 24 hours at 1500°C and $p_{O_2}=4.76\times10^{-7}$ atm, Mn content determined by chemical analysis is 3.20 mass per cent). 300

1 INTRODUCTION

1.1 History and uses of manganese and ferromanganese alloy

Manganese ores have been used since ancient times in the glass and ceramic industries to glaze the surface of pottery in brown. In spite of its long uses in the history, only in the late eighteenth century, the European iron and steel makers became interested in manganese metal for the production of steel. By the middle of the nineteenth century, manganese had already assumed great importance and helped to make the Bessemer process possible by acting as a deoxidizer and desulphurizer as well as improving the rolling properties of the metal. Towards the end of the nineteenth century, manganese was considered seriously as an alloying element to improve the strength, workability, toughness, hardness, abrasion resistance and response to heat treatment of a wide variety of steels.

Manganese is probably the most versatile additive in the steel industry and has the added advantages of easy availability and low cost. A major use is as an alloy addition to steel where it acts as a desulphurizer and deoxidizer as well as providing improved rolling and forging characteristics together with strength, hardenability, wear resistance via suppressing the hardening transformation of steel on quenching. It is also added to aluminium, silver, magnesium, copper, titanium, nickel, and zinc alloys as an alloying element. In some alloys, special properties are developed, such as

high damping capacity, high permanent magnet characteristics (BiMn, AlMn), low expansion and high electrical resistivity[1].

Manganese can be added in the form of its ore during iron-making, or as ferromanganese alloy in the steel-making stage. High carbon ferromanganese is the most common alloy used as an additive to steel. On the other hand, ferromanganese silicide and low to medium carbon ferromanganese have a suitable proportion of the alloying addition used in order to produce steels with low carbon contents.

Although titanium and zirconium are relatively effective agents for desulphurizing iron and steel, and although alloying elements nickel, chromium and molybdenum impart to steel some of the same physical properties as manganese, these elements are not considered interchangeable due to their properties which may or may not be desired or needed in the final steel, and are generally more expensive. Therefore, manganese occupies a unique position among the other alloying elements and its consumption in the world exceeds all other ferroalloys combined.

There are three main types of ferromanganese alloys:
-High carbon ferromanganese,
-Ferromanganese silicide and,
-Low to medium carbon ferromanganese

Table I shows the composition limits for these alloys. The major producers of high carbon ferromanganese are the former U.S.S.R., U.S.A., Japan and South Africa[2].

Ferromanganese silicide is another alloy used both as an addition to crude steel and as an ingredient for the production of low to medium carbon ferromanganese. The main producers of this alloy are Japan, U.S.A. and Norway. Low carbon alloys are needed as additions to blown steel for the production of thinner finished steel products. The major producers are Japan, U.S.A., France and South Africa[3].

In chemical industry, manganese is used as an oxidizing agent for dyes, flavours, fragrances and sealants and for production of chemical compounds. Manganese compounds are used in glasses, pigments, porcelains, colouring agents for glazes, preservatives for foods, dyes in paints, bleaches for textiles and to increase tackiness in rubber as well as in the production of fireworks and matches. One of the most important single application of manganese compounds is in the dry battery industry where manganese oxide is used as a depolarizing agent. Manganese is also used as a constituent of medicines, fungicides, fertilizers as well as a food stock additives since it has nutritional value as a trace element. Manganese chemicals are also used in environmental applications i.e. water treatment, air pollution control, fuel additives and in hydrometallurgy for example in uranium and zinc processing[4].

Since manganese is used mostly as a ferroalloy for additions to steel during melting, the commercial production of ferroalloys from manganese ores constitutes an important branch of the metallurgical industry. The manganese may be obtained from a number of sources which include manganiferrous iron ore for use in the blast furnace, spiegeleisen or a low grade ferromanganese, medium-carbon ferromanganese, low-carbon ferromanganese, silicomanganese. Manganese metal is being increasingly used instead of low-carbon ferromanganese in the production of stainless and alloy steels with very low carbon contents[5].

Table I. Compositions of different ferromanganese alloys[3].

Alloy	Composition (%)			
	Mn	Fe	Si	C
High carbon	74-82	12.2-19.9	0.1-0.8	6-7
Ferromanganese silicide	65-75	19.6-Bal.	15-32	0.4-2.3
Medium carbon	80-85	11-18	1-2	1-2
Low carbon	80-85	13.5-18.5	1.0	0.5

1.2 Manganese ore in the world and in South Africa

Manganese deposits are distributed throughout the world and total reserves are estimated at over two billions tons. The former U.S.S.R. has the largest deposits in the world which accounts for more than 50 per cent, the largest deposits being in the Chiatura and Nikopol areas. The manganese ore production in South Africa is estimated

to be the second largest in the world[1] (Table II). The manganese ore was originally mined in South Africa at Hout Bay, near Cape Town, and in 1917 small quantities were exported. The most important manganese occurrences in South Africa, however, lie in the Northern Cape province. These deposits extend from Postmasburg northwards through Sishen, Hotazel and Severn to Botswana border, a distance of 350 km. A gap of 55 km separates them into the southern field and northern (Kalahari) field. The Postmasburg and Kalahari or Kuruman fields are considered to be linked, although there are many differences in detail and geology between them. The ore in the Kalahari is continuous from the Mamatwan mine to the Wessels mine in the north and only a few isolated erosion remnants occur as islands on the north of the Wessel mine. The estimated values for the reserves in the Kalahari manganese deposit are seen in Table III.

Mamatwan mine is the largest open-cast mine in the Kalahari field and it was opened in 1963. However, Wessel mine is the largest underground mine in the Kalahari field. These fields differ in type of ore body, stratigraphic position and genesis[6].

Table II. World production of manganese ore (in million short tons)[1].

Country	Mn%	1980	1970	1960
Brazil	38-50	2.60	2.07	1.10
Chile	33-40	0.03	0.03	0.05
Hungary	30-33	0.09	0.18	0.14
Italy	22 +	0.01	0.066	0.06
The former U.S.S.R.	35	10.75	7.54	6.47
Turkey	35-46.6	0.05	0.01	-
Bulgaria	30 +	0.05	0.04	-
Yugoslavia	30 +	0.03	0.02	-
Gabon	50-53	2.36	1.60	-
Ghana	30-50	0.28	0.45	0.60
Morocco	50-53	0.15	0.12	0.53
South Africa	30-48+	6.28	3.57	1.32
Zaire	30-57	0.02	0.38	0.42
China	20 +	1.15	1.10	1.32
India	10-54	1.81	1.82	1.32
Japan	24-28	0.09	0.29	0.36
Thailand	46-50	0.06	0.03	-
Australia	37-53	2.16	0.83	0.07

Table III. Estimate of reserves in the Kalahari manganese deposit[7].

Wessels grade (Mt)					Mamatwan grade (Mt)			
+44	Mn%	(60 % (Mn + Fe))	=	330	38-40	Mn%	=	982
40-44	Mn%	(60 % (Mn + Fe))	=	30	30-38	Mn%	=	6284
36-40	Mn%	(60 % (Mn + Fe))	=	18	20-30	Mn%	=	5938
30-40	Mn%	(5-10 % Fe)	=	31				
		Subtotal	=	409	Subtotal		=	13204
Total reserve = 13613 Mt (based on data from approx. 1337 boreholes								

1.3 Production of carbon bearing ferromanganese

1.3.1 Production methods

High-carbon ferromanganese is commonly produced both in blast furnaces and in electric smelting furnaces by employing carbon as reducing agent. The electric smelting furnace has several advantages over the blast furnace due to its easier operation, increased flexibility and less coke requirement. Another advantage of electric smelting furnace is that the purity of the alloy produced is higher. Two processes are employed in the manufacture of high-carbon ferromanganese in the electric furnace. They are referred to as the low- (discard) and high- (enriched) slag practice.

The low slag practice is the least economical in terms of production costs per ton of ferromanganese and it produces the normal grades of high-carbon ferromanganese. The slags produced contain 8 to 15 per cent MnO and they are discarded. This practise is employed when the manufacturer does not produce silicomanganese for which a slag of higher manganese

content can be used as a raw material or has no sale for the higher manganese bearing slag. On the other hand, the time taken for extraction of manganese is 20 per cent higher than that of the high slag practice. In this case, the Mn-to-Fe ratio is also higher due to the more manganese extracted. This is important for the manufacturer when the Mn-to-Fe ratio of the ore used is low.

MnO in the slag acts as a flux and the decreasing amounts of MnO for a given burden requires the additional flux as CaO and MgO in order to maintain the required slag basicity. Since this slag is discarded, the recovery of manganese in useful product is only about 80 per cent.

In high slag practice, the slags produced contain between 25 and 40 per cent MnO. This slag is used in the production of silicomanganese alloys due to their extremely high Mn-to-Fe ratio and low phosphorus content. The total manganese recovered in useful products range from 94 to 98 per cent depending on whether the furnace has an open or a closed top. Total manganese removed as high-carbon ferromanganese and silicomanganese will approximate to 90 per cent. This recovery is much higher than that of the low slag practice.

1.3.2 Manganese oxide and their reduction reactions

Manganese can exist as the oxides MnO_2, Mn_2O_3, Mn_3O_4 and MnO. However, manganese(II) oxide plays an important role in the reduction process as higher manganese oxides

dissociate and are reduced in the solid state at relatively low temperatures. Therefore, manganese oxide (MnO_2) is stable up to 425°C, but above this temperature it is transformed into manganese(III) oxide according to the following equation:

$$2MnO_2 = Mn_2O_3 + 1/2O_2 \quad \text{.....(1)}$$

Manganese(III) oxide dissociates at 950°C to manganous oxide as follows:

$$3Mn_2O_3 = 2Mn_3O_4 + 1/2O_2 \quad \text{.....(2)}$$

At 1172°C, Mn_3O_4 transforms entirely into manganese(II) oxide:

$$Mn_3O_4 = 3MnO + 1/2O_2 \quad \text{.....(3)}$$

Also some of the higher manganese oxides are reduced to lower oxides with the CO of the furnace gases, comparable with iron oxide reduction in the electric pig iron furnace. The reduction of MnO to Mn by this means is theoretically unlikely with the conditions prevailing in the furnace. The reactions with CO may be expressed as belo

$$2MnO_2 + CO = Mn_2O_3 + CO_2 \quad \text{.....(4)}$$

$$3Mn_2O_3 + CO = 2Mn_3O_4 + CO_2 \quad \text{.....(5)}$$

$$Mn_3O_4 + CO = 3MnO + CO_2 \quad \text{.....(6)}$$

At the reaction zone temperatures, it is possible to consider the reduction reaction to metal as follows:

$$MnO + C = Mn + CO \quad \text{.....(7)}$$

$$3MnO + 4C = Mn_3C + 3CO \quad \text{.....(8)}$$

The theoretical initial temperatures of these reactions (7) and (8) are 1420° and 1223°C respectively, indicating that reduction down to Mn_3C is the most likely and explains why it is impossible to obtain ferromanganese of low carbon content using carbon as the reducing agent.

On the other hand, the reactions occurring may be complex and variable. The manganese in ores is not present entirely as free oxides but often as complex silicates, carbonates, and other compounds, and is closely associated with clay, bauxite and other minerals. The decomposition of manganese ores in actual furnace

operations is affected by the conditions and the temperature ranges. The rate and degree of dissociation are therefore variable, and, as such, a function of the composition and also the physical characteristics of the ore used. The temperature at which the ores begin to soften, and the temperature of primary slag formation, affect the properties of the slags produced.

Tyslev[8], studied the ferromanganese blast furnace processes and found that only solid phase is found in the range of temperature from 750° to 800°C. At this temperature range, pyrolusite (MnO_2) is reduced to haussmanite (Mn_3O_4) and evolution of chemically combined moisture takes place. At 800° to 900°C the ore begins to sinter and passes into the initial stage of the plastic state where any minerals such as $MgO.Fe_2O_3$, $2CaO.Fe_2O_3$, $2CaO.SiO_2$, $3CaO.2SiO_2$, $MnO.Al_2O_3$, $MnO.Fe_2O_3$, $CaO.MgO.SiO_2$, etc. are formed due to the recrystallization of the original material. By this stage the higher oxides of manganese are almost completely decomposed or reduced to MnO.

Slightly higher temperatures leads to the formation of the liquid phase as determined by manganese monticellite ($2CaO.SiO_2.2MnO.SiO_2$) and other silicates. The melting temperature of these silicates is exceeded before reduction of the manganese(II) oxide is started due to the high temperature required for MnO reduction. Finally, the final reduction is accomplished by the interaction of solid carbon with a liquid slag containing MnO. The extent to which MnO can be reduced depends on the other constituents in this slag.

By the time the temperature reached has 1100°C, the liquid state is the predominant phase although some of the components are in the plastic state as they pass only slowly into the liquid. In a blast furnace, it is desirable to have this range between softening and melting as small as possible as this region offers the highest degree of resistance to penetration by gases in order to ensure smooth operation of the furnace.

As the primary slag descends in the furnace it takes up and dissolves CaO, MgO, Al_2O_3 and SiO_2 from the ore (gang) and ash from the reducing agent. The dissolution of the basic components free the MnO from the silica network and MnO reacts with carbon to form manganese carbide.

At this stage, most of the iron oxide would have already been reduced by the action of solid carbon as well as by CO from the furnace gases. The iron carbide thus formed accelerates the reduction of MnO from the slag through the reaction:

$$3MnO + 4Fe_3C = Mn_3C + 12Fe + 3CO \quad \text{.....(9)}$$

This reaction takes place as the iron carbide descends as small globules through the slag layer. At higher temperatures, silica is also reduced with solid carbon and this also reacts with MnO in the slag by the following reaction:

$$2MnO + Si = SiO_2 + 2Mn \quad \text{.....(10)}$$

Therefore, it can be summarized as such that manganese(II) oxide (MnO) is reduced by three agents which are iron carbide, reduced silica and solid carbon. Reduction by solid carbon is believed to be the most important.

1.4 The motivation of the present study

Almost without exception, the slag is an essential phase in metallurgical operations. Only relatively recently have the nature of slag-metal reactions and the relationships between properties, composition and temperature of liquid oxides been somewhat understood to put the technology of slag control in a metallurgical operation on a scientific basis.

Currently most manganese-containing alloys are produced by reducing manganese ores in electric furnaces. Because manganese is a strategic and critical material and because it is under competition, the optimization of the recovery of manganese in smelting and refining processes is essential. In other words, it is necessary that the ferromanganese smelting process be efficient and from physicochemical point of view, the efficiency depends, in part, on the distribution of the valuable manganese among the alloy, slag and gas phases which, in turn, depends on the thermodynamic properties of the alloy and slag phases and the phase equilibria among them. One can say that the efficiency of the ferromanganese smelting

process is governed to a large extent by the thermodynamic activities of MnO in the slag and that of Mn in the alloy phase from a scientific point of view. Such knowledge, when coupled with liquidus temperature, viscosity and electrical conductivity information, is extremely useful in maximizing the efficiency of the process, in predicting the changes that may occur due to use of somewhat different raw materials and changes in furnace operation. On the other hand, the literature on thermodynamic activity of MnO in ferromanganese type of slags is scarce, incomplete and very limited. Although a substantial amount of data has been available on the binary SiO_2-MnO system and on ternary CaO-SiO_2-MnO, MgO-SiO_2-MnO systems, more complex systems have not been investigated. Furthermore, it is felt that the data provided are not accurate enough due to discrepancies in standard free energy of formation of MnO and $xMnO.ySiO_2$ compounds that existed at the time when these experiments were conducted. Therefore, it is clear that measurement of thermodynamic activity of MnO in ferromanganese slags and the slag-metal equilibrium distribution of certain elements, such as silicon and manganese are important, both to plant metallurgist and scientists. Furthermore, when a complete set of data has been accumulated, these can be stored in a data bank for use whenever necessary such as for new process development. From an academic point of view, determination of these physico-chemical properties is also extremely important to predict and understand the behaviour, structure and property relationships of slag and metal phases.

Since the South African manganese industry began in Newcastle in 1937, enormous developments have taken

place in terms of production capacity and methods. However, in spite of the new methods applied in the submerged-arc electric furnace which is major tool for the production of the ferromanganese alloy today, the efficiency of the recovery of valuable manganese is not optimum due to the loss of manganese to the slag and more efficient methods which will increase the efficiency must be found and improved as the new alternatives.

Although manganese is critical, strategic and important material, due to the decline in the world production of steel, it is under heavy competition globally. Ferromanganese production must be efficient and cost-effective in order to remain competitive in the global market. Therefore, creating new utilization fields for manganese and its alloys has great importance bearing in mind that the production must be cost-effective. Furthermore, the ferromanganese slags with high MnO contents are too valuable to discard. On the other hand, deposits of high grade manganese ore are being depleted and in the future, it will be necessary to use lower grade ores such as Mamatwan ore from Postmasburg region of the Cape Province.

Therefore, as mentioned above, knowledge of slag-metal equilibria in the system relevant to ferromanganese production is a fundamentally important and vital stage in the understanding of pyrometallurgical processes for the smelting of ferromanganese ores. Once slag-metal equilibrium distribution of important elements is known,

some of the problems encountered in smelting, like manganese losses to slag, can be predicted and deviations from equilibrium can be handled.

This laboratory scale research work was undertaken to study the thermodynamic activity of manganese oxide in ferromanganese slags and the distribution of manganese and silicon between metal and slag phases. The aims of the study can be summarized as:

-The determination of Mn activities in Pt-Mn binary alloy system,

-The determination of MnO activities in synthetic ferromanganese slags with compositions similar to those encountered in ferromanganese production in South Africa,

-to study the equilibrium distribution ratios between metal and slag phases,

-to develop an empirical model equation based on the present MnO activity data to predict the MnO activities in the composition range studied.

Consequently, a better understanding of behaviour, structure and property relationships of the slag and metal phases through thermodynamics would result in a better understanding of the operation. Furthermore, the recovery of manganese could be optimized.

2 LITERATURE SURVEY

2.1 General considerations

A quantitative understanding of the role of manganese oxide in ferromanganese slags, and of the distribution of elements such as manganese and silicon between metal and slag phases, requires a knowledge of the activity-composition relations of manganese oxide in these phases.

Literature on thermodynamic activity of MnO in ferromanganese type of slags is very limited, although a substantial amount of data has been accumulated on the binary SiO_2-MnO system. MnO activities in blast furnace type slags and in CaO-SiO_2-MnO and MgO-SiO_2-MnO ternary systems have also been determined, but it is probable that the data provided are not very accurate due to discrepancies in standard free energies of formations of MnO and $xMnO.ySiO_2$ compounds that existed at the time when these experiments were conducted. On complex systems similar to ferromanganese slags, only one study has been done[9]. However, it was found that MnO activities were not available in the range of slag compositions that would be of interest to ferromanganese producers in South Africa.

In order to measure the activities of MnO by the gas equilibration technique in ferromanganese slags, it was necessary to redetermine the activities of manganese in

its solid alloys with platinum at the temperatures around 1500°C. A number of investigations were done in the past on thermodynamics of Pt-Mn alloys[10-12]

The knowledge on the distribution of elements like manganese and silicon between slag and metal phases is fundamentally important to be able to optimize the smelting process in ferromanganese production. The manganese losses to the slag can be estimated and the deviations from equilibrium can be controlled by making use of this knowledge. Slag-metal reactions are redox exchange reactions which take place by an exchange of electrons between the reacting species as they are transferred to and from non-polar metallic phase and ionic molten slag. These reactions are, in principal, identical to gas-slag reactions with regard to the exchange of electrons. In most cases the transfer of a reactant from metal to slag is an oxidation process, such as:

$$Fe + O = Fe^{2+} + O^{2-} \quad \text{.....(11)}$$

$$Mn + O = Mn^{2+} + O^{2-} \quad \text{.....(12)}$$

Although the reactions as formulated above are conceptually correct, their equilibrium constant can not be evaluated because the thermodynamic activity or activity-coefficient of an individual ion cannot be determined experimentally, for the same reasons which

preclude the determination of activities of ions in concentrated aqueous solutions[13]. Although the derivation of reaction-equilibrium relations from an ionic structural model is of theoretical interest, their application to slag-metal equilibria in multi-component systems has not been particularly rewarding when compared with the much simpler conventional methods of representing the slag-metal equilibria in terms of the measured thermodynamic quantities.

The knowledge of the activities of slag components are always useful when a slag is involved in a chemical reaction. Values of these activities have been difficult to obtain, because their determination requires difficult high temperature experimentation and very accurate chemical analyses. The range of interest lies often between the Rault's law and Henry's law ranges, and suitable standard states are not always easy to specify in such strong solutions. Because of lack of activity data for multi-component slags, the slag-metal equilibrium relations are often represented in terms of concentration of reactants and products by invoking the mass-action law. The isothermal equilibrium constant K thus expressed varies with the slag composition, when the activity-coefficients of oxide reactants and products in the expression of the equilibrium constants are omitted.

The composition dependence of activities in polymeric melts is related in a general way to changes in state of depolimerization of the melt with composition[14]. Although qualitative, the slag basicity defined by the concentration ratio (oxides of network modifiers) :

(oxides of network formers) gives a general indication of the extent of depolimerization of the melt, and hence is a simple indicator of the trend in changes of oxide activities with composition. Consequently, the equilibrium constants for slag-metal reactions, expressed in terms of concentrations of slag components, are often simple functions of slag basicity, at least for composition ranges of practical interest.

2.2 Pt-Mn binary system

The activities of manganese in solid platinum at temperatures of 1500 and 1650°C have been first determined by Abraham and his co-workers[10]. The technique adopted was to measure the manganese taken up by solid platinum (solid solution), when brought into equilibrium with pure manganese oxide at controlled partial pressures of oxygen, ranging from 10^{-7} to 10^{-3} atm, nine hours were required to bring the platinum to equilibrium with the solid oxide at both temperatures mentioned above. Consequently, the experiments were normally run for periods of 9-12 hours. Abraham and his co-workers employed reaction (13) in order to determine the activities of manganese in solid platinum and the values of activity coefficient of manganese were calculated by application of the equation (14) derived from the equation (13). The round brackets indicate oxide components and square brackets indicate components in the metal phase.

$$[Mn] + \frac{1}{2}O_2 = (MnO) \quad \text{.....(13)}$$

$$\log\gamma_{Mn} = \log\frac{a'_{MnO}}{\sqrt{p'_{O_2}}X_{Mn}} + \frac{\Delta G^0}{2.303RT} \quad \text{.....(14)}$$

In equation (14), p'_{O_2} is the partial pressure of oxygen and a'_{MnO} is the activity of stoichiometric MnO in the oxide which is non-stoichiometric when p'_{O_2} exceeds 10^{-9} atm, ΔG^0 is the free energy of formation of one mole of stoichiometric MnO from solid manganese and oxygen. The ΔG^0 values were derived by extrapolation above 1244°C[10] of the ΔG^0 values calculated by Coughlin. The a'_{MnO} values were measured at different p'_{O_2} levels in a previous study carried out by Davies and Richardson[15] and by employing these values in equation (14), the non-stoichiometry of MnO was handled.

$\log\gamma_{Mn}$ is shown as a function of composition in Figure 1. As it is seen in Figure 1, a linear relationship was found between $\log\gamma_{Mn}$ and X_{Mn}.

The following work by Smith and Davies[11] was carried out to apply the Pt-Mn activity data of Abraham, Davies and Barton[10] to the determination of MnO activities in CaF_2-based slags, largely by use of Abraham, Davies and Richardson's technique[10]. However, Smith and Davies[11] obtained anomalous results which have led to a redetermination of the activity of manganese in platinum at 1500°C, and 1600°C. The experimental technique described by Abraham and his co-workers[10] was employed with following differences. A $CO-CO_2$ gas mixture was used instead of $H_2-CO_2-N_2$ and the majority of the

experiments were carried out with CaF_2-MnO slags saturated with MnO. Several experiments at an oxygen potential of 10^{-5} atm and 1600°C were carried out with pure solid MnO as a check on the CaF_2-MnO experiments. Runs were of 12 hours duration using the CaF_2-MnO slags. Although it was found that equilibrium was reached under 6 hours for slags, for the solid MnO experiments, it was found necessary to hold for 17 hours before equilibrium was reached. This was in contrast to the experience of Abraham and his co-workers[10].

The equations (13) and (14) were employed in order to calculate the Mn activities in binary Pt-Mn alloys. ΔG^0 values were derived by extrapolation above 1244°C[11] of the ΔG^0 values, as given by Coughlin and a'_{MnO} values were taken from Davies and Richardson[15]. Smith and Davies[11] also used the alternative data in order to calculate a'_{MnO} values as a check on the a'_{MnO} values and found a numerical difference of less than 3 per cent on a'_{MnO} even in the case of maximum discrepancy. a_{Pt} values were obtained by a Gibbs-Duhem integration. The equilibrium manganese levels were compared with those of Abraham and his co-workers[10] as it is seen in Figure 2. At 1500°C there is a small difference between values of Abraham et al. and the values of Smith and Davies[11] but at 1600°C, the results nearly coincide with results of Abraham et al. at 1650°C . There was no explanation for the discrepancies. Thus, they draw attention to the use of MnO-saturated CaF_2 slags that if solid solution existed between MnO and CaF_2, or if hydrolysis of CaF_2 led to the presence of CaO, a'_{MnO} values would be reduced and the discrepancy would be in the opposite direction. However, they obtained a value of a'_{MnO} greater than unity when they applied the

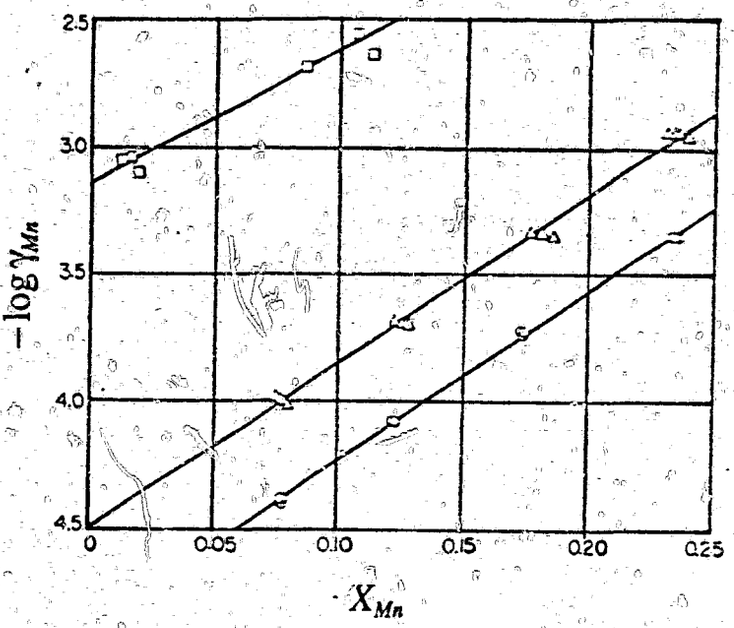


Figure 1. The activity coefficient of solid manganese measured by Abraham et al.[10] in solid Mn-Pt alloys at 1500° and 1650°C. The top line shows on the same scale, values for the activity coefficient of liquid iron in solid Fe-Pt alloys at 1550°C as measured by Larson and Chipman.

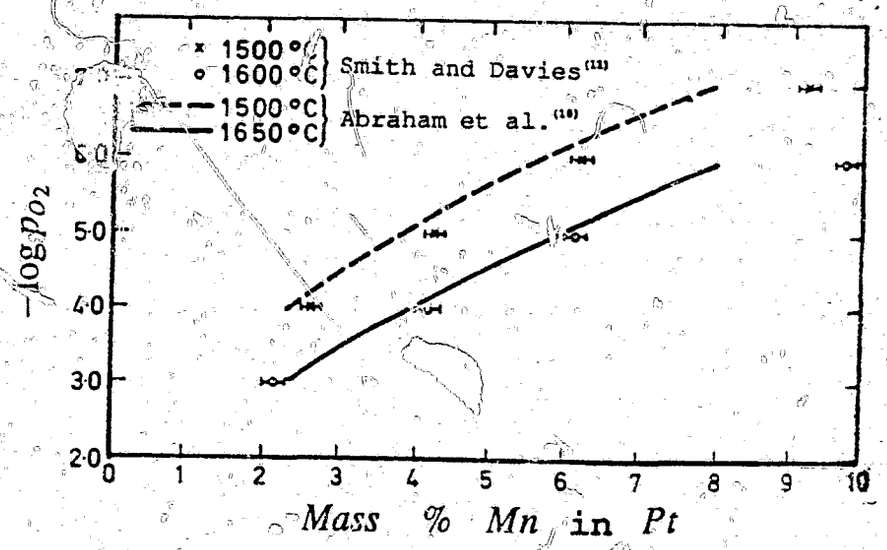


Figure 2. Equilibrium concentration of Mn in Pt-Mn alloys[11].

Pt-Mn activity data of Abraham et al. in order to calculate the MnO activities in MnO-saturated CaF_2 slags. Furthermore, the experiments designed to compare the use of solid MnO gave exactly the same results within experimental error, although it was observed that considerably longer times were required to reach equilibrium than those quoted by Abraham and his co-workers[10].

In a later study, Rao and Gaskell[12] obtained anomalous results when they used the data of both previous studies[10,11] in evaluating MnO activities in various binary and ternary slags. Therefore, the activity of manganese in Pt-Mn alloys were redetermined in the temperature range 1300°-1600°C in the composition range $0.07 \leq X_{Mn} \leq 0.33$ by equilibrating platinum foils with solid MnO under atmospheres of fixed oxygen pressure obtained by using CO-CO_2 mixtures. The results obtained were different from those of the two previous investigations of this system[10,11]. The reaction (13) was employed and the Mn activities were calculated through the equation (14) as in two previous studies[10,11]. Abraham and his co-workers[10] found $\ln\gamma_{Mn}$ to be linear function of X_{Mn} in the range $0 \leq X_{Mn} \leq 0.2$ and Smith and Davies[11] found $\ln\gamma_{Mn}$ to be an approximately linear function of X_{Mn}^2 in the range $0 < X_{Mn} < 0.28$. Rao and Gaskell fitted their data, in the experimental composition range, into the expression below:

$$\ln\gamma_{Mn} = a_0 + a_1 X_{Pt}^2 + a_2 X_{Pt}^3 + a_3 X_{Pt}^4 \quad \text{.....(15)}$$

The results of Rao and Gaskell[12] are seen in Figures 3 and 4. In Figure 3, the variation of the equilibrium manganese contents of the alloy with oxygen pressure and temperature are shown. In Figure 4, the variations of $\ln\gamma_{Mn}$ with temperature and composition are shown. In Figure 5, the results of three studies on Pt-Mn system are shown. The solid line represents the results of Rao and Gaskell and the symbols represent the two previous work[10,11]. As it is seen in Figure 5, the results of Abraham et al. are in better agreement with those of Rao and Gaskell. An explanation for the differences among the results of these three investigations can not be offered.

2.3 Structure and properties of slags

Slag is a generic term used to designate a great variety of simple and complex compounds, which may be solutions of oxides from different sources, sulphides from the charge of fuel and, in some cases, halides such as CaF_2 which are added as flux. In high temperature metallurgical operations, slag forms a non-metallic bath, due to its immiscibility and low density. By comparison with molten metals, liquid slags show great diversity of properties, capable of wide variation according to chemical composition and temperature. The reason lies in the equal diversity of structure. From a metallurgical point of view, interest is directed almost exclusively at the properties of a slag in its liquid state.

The primary function of a slag is to serve as a receiver for the unwanted liquid and solid constituents of the

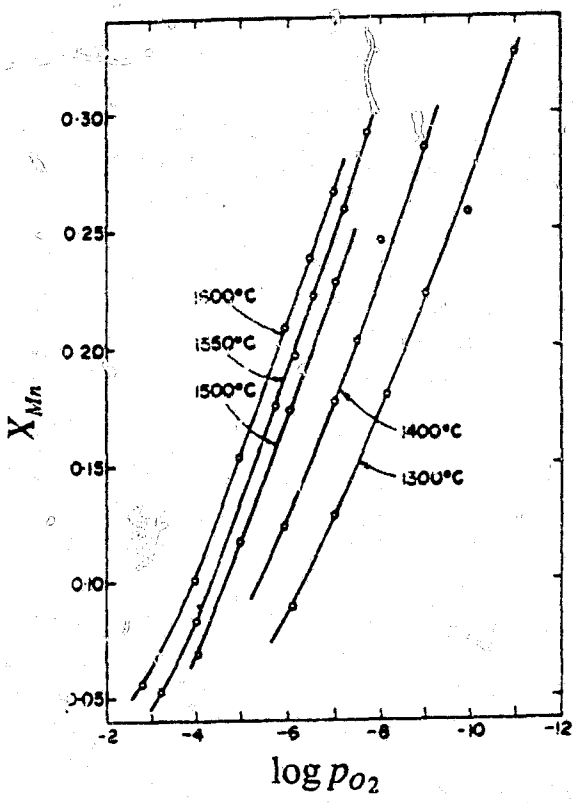


Figure 3. The variation with temperature and oxygen pressure of the Mn content of Pt-Mn alloys equilibrated with solid MnO[12].

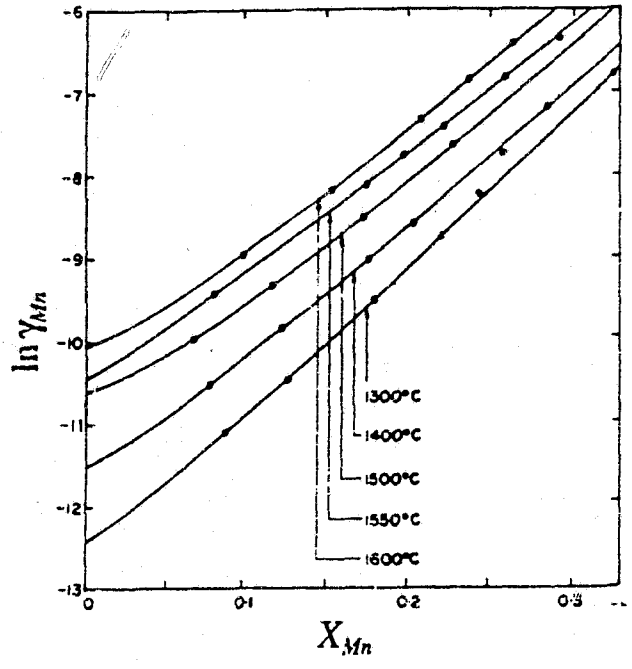


Figure 4. The variation with temperature and composition of $\ln \gamma_{Mn}$ in Pt-Mn alloys[12].

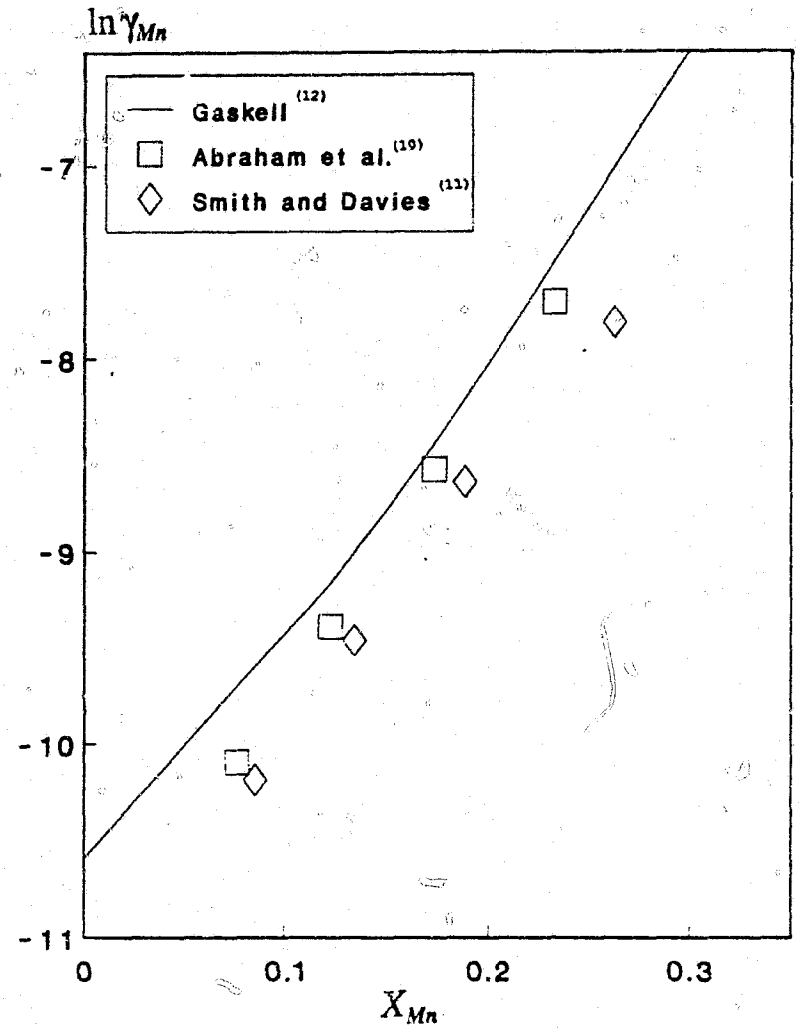


Figure 5. The variation of $\ln\gamma_{Mn}$ with composition in Pt-Mn alloys studied in three previous studies[10,11,12].

metal bath, including the gangue from the valuable ores and the elements which are partitioned between the metal and the slag phases. Therefore, the composition of a slag must often be adjusted within narrow limits to secure an optimum removal of the undesirable elements without removing other elements required in the metal. The slag may be required also to fulfil other needs, such as controlling the supply of oxygen from the atmosphere into the metal, or to act as a physical barrier to the passage into the metal of gaseous species such as hydrogen, nitrogen and sulphur. The formation of a liquid slag from solid oxides is endothermic and generally the thermal efficiency of the process is related inversely to the volume of the slag. In some processes, heat is supplied from the metal bath, as in the open-bath electric-arc furnaces, so that the slag acts as a thermal barrier and the rate of rise of the metal temperature is inversely proportional to the thickness of the slag layer.

Slags are capable of dissolving small amounts of neutral metal atoms, presumably lodged in the holes in the slag structure. They can also dissolve water in some form, probably dissociated; and can pass either oxygen or hydrogen or both from a furnace atmosphere through to a melt below[13]. The transmission of oxygen is very easy in the case of a slag containing iron oxide, or the oxide of any other metal which can display more than one valency.

The most common rate controlling factors for a reaction between the slag and the metal are the diffusion of the reacting species in the slag and the transfer of the

species across the slag-metal interface, so the viscosity and the surface tension of the slag are also of considerable importance. In the electric smelting furnace, the slag is frequently used as a resistor.

To achieve their functions adequately, slags must have certain physical (melting point, electrical conductivity, viscosity) and chemical (basicity, oxidation potential, thermodynamic) properties. They must have sufficient fluidity to run freely when they are removed as a liquid from the furnace and have ability not to decrease the rate of mass transfer to and from the slag-metal interface. They must become fluid at a low enough temperature for the process to be worked economically with as little heat input and refractory wear as possible. Fluxes such as lime, quartz, fluorspar or iron oxide may be added solely to lower the liquidus temperature and viscosity of slags. Their specific gravity must be sufficiently different from that of the metal to allow easy operation. They must have suitable composition and structure to dissolve impurities and gangue minerals at low activity and to allow any desired slag-metal reactions to occur[16-18].

2.3.1 Structure of silicate melts

The knowledge about the slag structure began with investigations into the structure of glass due to the result of two important facts. Firstly, a glass is essentially a non-crystallised rigid solid which can be considered to possess a "frozen-in" liquid structure[19,20]. Secondly, many glasses are derived from liquids which are slag-like both in their properties and in composition.

In terms of the molecular theory, the chemistry of slags was considered as solutions of component oxides in which certain acidic oxides are more or less completely held in combination with basic or metallic oxides, the nature of the interoxide compounds being derivable from the chemical behaviour of the slag or the mineralogy of the solidified specimens.

The measurements of the physical properties such as electrical conductivity[21], electron transport[22], viscosity[23], and expansivity[24] of the silicate melts have caused a marked change in the molecular theory proposed to represent the slag structures.

Investigations by Bockris and his co-workers[21-24] greatly extended the state of knowledge about the structure of the liquid slags. By showing that in binary alkaline and alkaline earth silicates:
(a) the electrical conductivity is of the same order of magnitude as for ionic melts, e.g. fused salts;
(b) the ratio of the conductivity above and below the liquidus temperature is about 100;
(c) the temperature coefficient of electrical conduction is positive;
(d) the passage of current through the melt produces electrolysis.
Bockris concluded that slags were ionic liquids and that electrical conduction was a cationic process. He added that the viscous flow process reflected the size and interparticulate attraction of the large constituents of the slag (the anionic silicate group). He suggested that viscosity measurements should therefore be a factor in

explaining slag structure. Considering viscosity, density, and compressibility measurements on liquid silicates, Bockris formulated his discrete ion theory of slag structure. He shortly proposed that the infinite random network would be progressively weakened by breakage of Si-O-Si bonds as basic oxides were added to pure silica. The individual stages of depolymerisation or dissociation, which overlap with one another was described as follows. At about 12 mole per cent basic oxides, this three-dimensional infinite network would break down into large, discrete ring structures. As the basic oxide content increased, the size of these discrete ions would decrease further until ring structures gave way to chain structures at about 50 mole per cent basic oxides. At the orthosilicate composition (66 mole per cent basic oxide) only SiO_4^{4-} ions exist and further additions of basic oxides would introduce free oxygen ions (O^{2-}).

The discrete ion theory was not found to be adequate to describe molten silicate systems especially from a thermodynamic point of view. Meadowcroft and Richardson[25] modified the theory and so provided the basis for understanding of the structure of liquid slags. Their new idea was based on work done on binary and ternary phosphate systems which, from many points of view, were analogous to binary silicates. They used the existing chromatographic techniques for the extraction of polyphosphate ions from phosphate glasses. They found that in the liquid state there existed a continuous distribution of ions of increasing weight and size as opposed to the few discrete ions proposed by Bockris. Therefore, Meadowcroft and Richardson[25] proposed that in

silicate systems similar polymerisation/depolymerisation reactions occurred and that the system was in a state of dynamic equilibrium. He expressed the network forming/breaking reaction in terms of an equilibrium

$$O^0 + O^{2-} = 2O^- \quad \text{.....(16)}$$

Thus, combination of any bridging oxygen (O^0) with a neighbouring free oxygen (O^{2-}) produced two non-bridging oxygens (O^-) and constitutes a depolymerisation process and a decrease in the size of polyanions. The reverse step constitutes polymerisation and an increase in the size of the polyions. Thus, increasing the proportion of basic oxides decreases the average size of the polyions and vice versa. The nature of the cations in the melt influences reaction (16) through control of the electronic environment at individual reaction sites. At present, the slag theory is not yet in a position to describe this influence in detail. The modern slag theory provides more satisfactory explanations for certain features of slag systems than was previously possible and also justifies the general features of the observations made by Bockris.

Direct studies of binary silicate melts by X-Ray diffraction at high temperatures were reviewed by Waseda[26]. X-Ray diffraction measurements on the molten and glassy binary silicates containing alkaline oxides in the composition range 0-60 mole per cent have shown

that the silicates mainly consist of SiO_4 tetrahedral units and the structural change in the fundamental units due to the addition of alkali metal oxide is insignificant. These SiO_4 tetrahedral units distribute more randomly with increasing addition of metal oxides. It was concluded that the existence of discrete SiO_4 tetrahedra becomes important at silica contents less than the orthosilicate composition, with polimerization to form chains and rings at higher silica contents.

Structural studies of glasses by Mossbauer spectroscopy have been reported by many investigators. Systems of metallurgical interest have been reviewed by Bowker, Lupis and Flinn[27]. Most of the slags studied were based on the system $CaO-Fe_2O_3-SiO_2$. The method was valuable for determining the changes in the state of valency and co-ordination number of iron. The works of several authors [28-30] showed that, in $Na_2O-CaO-SiO_2$ glasses, iron, at low concentrations, behaved as a network modifier in octahedral co-ordination with oxygen. Both Fe^{2+} and Fe^{3+} were able to occupy octahedral sites. An increase in the iron oxide content caused an increase in the fraction of Fe^{3+} in tetrahedral co-ordination and resulted in its taking a greater network forming role.

Infrared absorption spectra of $PbO-SiO_2$ glasses by Yanagase and Suginohara[31] showed a continuous shift in the $Si-O^-$ stretching vibration frequency to a lower wave number as the PbO content increased to 70 mole per cent as shown in Figure 6. Thereafter it remained constant at 890 cm^{-1}. This wave number was assigned to the vibrational mode of the SiO_4^{4-} ion and the continuous shift

was interpreted as due to a progressive breakdown of the silicate structure as PbO is added. The wave numbers corresponding to other compositions in the frequency-composition plot for $PbO-SiO_2$ were then used to make assignments for other glasses, as shown also in Figure 6. Thus, evidence was obtained for the presence of discrete ions or groupings at compositions corresponding to the formulae SiO_4^{4-}, $Si_2O_7^{6-}$, $Si_nO_{3n}^{2n-}$, $Si_{2n}O_{5n}^{2n-}$, $Si_{4n}O_{9n}^{2n-}$ and SiO_2^0

Furukawa, Brawer and White[32] studied the structure of $PbO-SiO_2$ glasses by Raman spectroscopy and attributed their results to depolimerization of the network. Orthosilicate ions began to appear at the metasilicate composition and their number increased gradually as the PbO content increased. However, depolimerization was not complete at the orthosilicate composition, implying that $Si_2O_7^{6-}$ and probably some larger groups were present. Piriu and Arashi[33] concluded that various discrete kinds of polymerized silicate units were present in basic melts and glasses of this system. The concentration of more polymerized units decreased in comparison with the less polymerized types as the PbO content increased. In addition, the decreasing frequency of the high frequency bands suggested that the mean chain length decreased with increasing PbO. These features were similar in both melts and glasses.

Raman and infrared spectroscopy were used by various authors to study the structures of silicate and

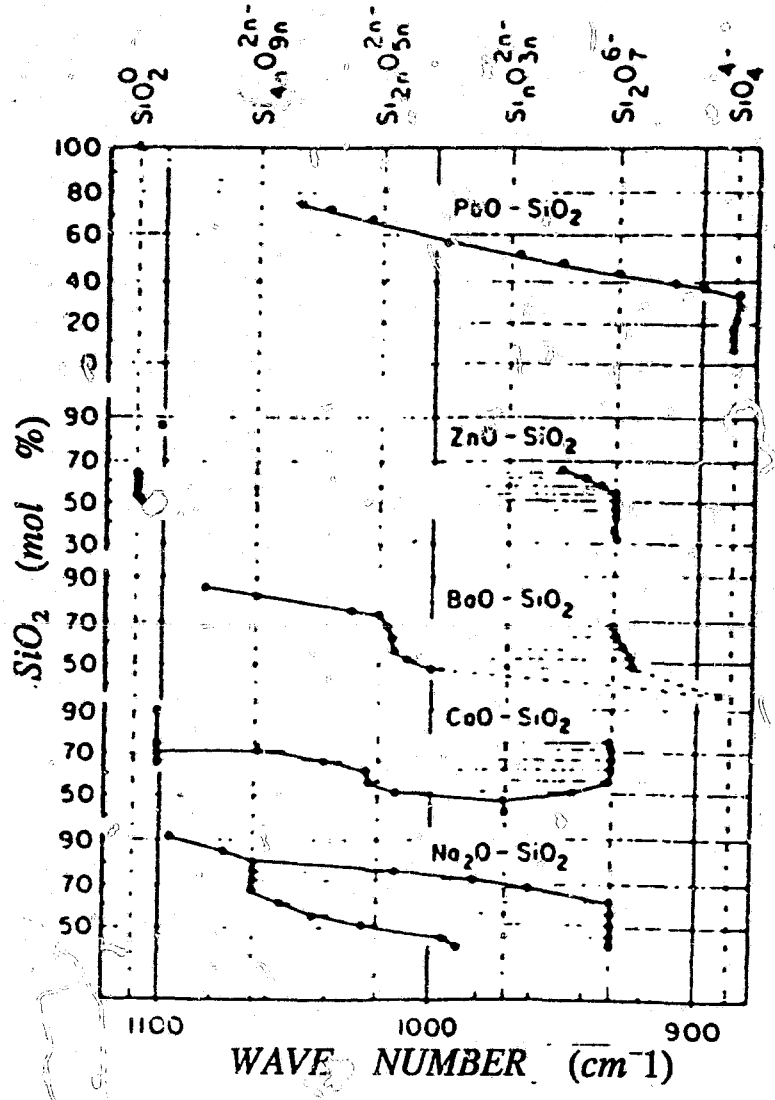


Figure 6. Relation between wave number of infrared absorption peak and SiO_2 content in binary silicate glasses[26].

aluminosilicate melts and glasses[34,35] and a large part of this work was devoted to understanding the structure of melts important in geological processes.

The alkali and alkaline earth silicate glasses were studied most intensively and their band systems were interpreted by comparison with spectra of corresponding crystals. This allowed the identification of band groups associated with the ortho, pyro, meta and disilicate compositions, and with vitreous silica. Mysen, Virgo and Scarfe[36] concluded that a very limited number of anionic structural units were present in silicate melts. These were considered to be monomers (SiO_4^{4-}), dimers ($Si_2O_7^{6-}$) chains ($Si_2O_6^{4-}$), sheets ($Si_2O_5^{2-}$) and three-dimensional network structures with four, three, two, one and zero non-bridging oxygens per silicate tetrahedron respectively. It was considered that any three of these could co-exist at a given composition.

Another Raman spectroscopic study on the structure of the glassy and molten states of the binary silicates was carried out by Iguchi and his co-workers[37]. For the first time, the results gave evidence for the co-existence of four different types of non-bridging oxygens. Therefore, this was a disprove to the accepted concept of regarding the non-bridging oxygens as single O^- ion alone.

The different techniques[38] as NMR spectroscopy, X-ray induced photoelectron spectroscopy (ESCA, XPS), and the technique of trimethylsilylation (TMS) were also used to

study the structure of silicate melts. Studies by many workers with crystalline materials of well-defined structure have shown that the TMS derivative of the parent material is usually obtained as the main product. The method was therefore valuable for identifying the major ionic species in materials of unknown constitution. Lentz[39], using TMS method showed that, in a 1 mole solution of sodium silicate with Na-to-Si ratio of 4, only 43.5 mass per cent of the silicon was present as SiO_4^{4-}, the remainder being dimer, trimer, and higher anions.

The direct evidence of the structure in the melt is very limited and this fact reflects the experimental difficulties which are involved in obtaining such data. But, there is some indirect evidence , such as the low values of entropies of fusion of oxides and the comparatively small change in viscosity on melting, which suggest that no major structural changes are involved on changing from the solid to the liquid state. Some information about the structure of a liquid slag can, therefore, be inferred from examination of the solid structures.

The solid oxide structure is relatively simple. The diagram of Si-O tetrahedra in crystalline and molten state is shown in Figure 7. Metallic cations are surrounded by oxygen ions in a three-dimensional crystalline network. Most of these oxides such as CaO, MgO, MnO and FeO form structure similar to that of sodium chloride, in which each cation is co-ordinated with six oxygen anions. This structure is called an octahedral

coordination and each oxygen ion is co-ordinated similarly with six cations. A few basic oxides exhibit an eight-fold co-ordination, but, in contrast, the co-ordination is only four-fold (or tetrahedral) for the cations in the acid oxides, silica, alumina and phosphorus penthoxide. The tetrahedral structure of silica are linked together to form a three-dimensional pattern of hexagonal cells. The structure of pure liquid silica is probably very similar, although the regularity of the solid lattice is distorted, and it can be regarded as a gigantic molecule (Figure 8). This hypothesis is supported by the fact that the viscosity of the liquid is very high because, in general, the viscosity is increased as the dimensions of the molecules are increased.

It has been widely accepted that the mechanism of slag-metal reactions in metallurgical processes is closely related to the chemical characteristics of complex silicate anions in the liquid state. Due to the fact that slags are associated with many of the most important processes of ferrous and non-ferrous extractive metallurgy, an understanding of their behaviour is essential to the control of these processes. For a better understanding of the slag structure, whenever possible, several techniques should be used to study the structure of slags in order to provide supporting and complementary information.

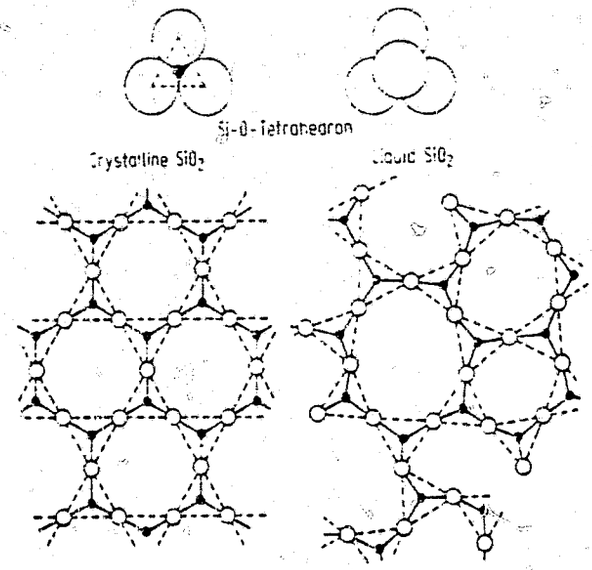


Figure 7. Diagram of Si-O tetrahedra in crystalline and molten silica.

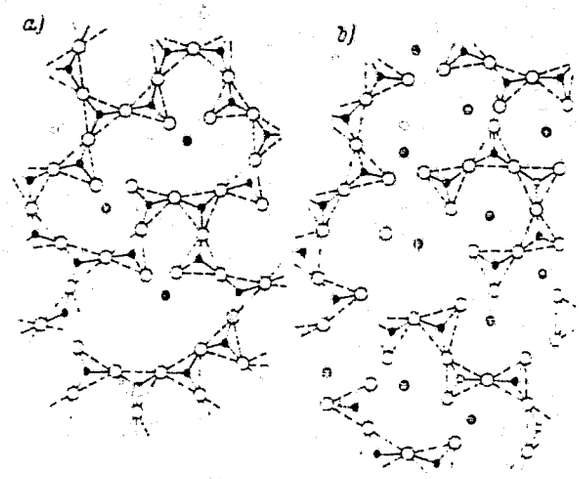


Figure 8. Diagram of dissolution of silica network by metal oxide.

2.3.2 Physical properties of slags

The physical properties of slags can be considered as density, viscosity, liquidus temperature, electrical conductivity and surface tension

The density of slags is an important property in the sense that the separation of the phases during the metallurgical processes is largely dependent on the density differences between the metal and slag phases. The density of a slag is a function of its composition[40], as an example, if a slag contains a high density oxide such as iron oxide, the density increases with increasing amount of this oxide. In another example, a slag containing calcium oxide has an increasing density with increasing amount of calcium oxide. Since the density of a slag is a direct measure for its volume, the densities of the slag systems can be determined from the molar volumes of the pure metal oxides constituting the slags[41]. Therefore, in a metallurgical process, by using the slag forming reactions in the ore+flux system, the volume of a slag can be determined from the amount and the composition of the fluxes used.

Viscous flow and electrical conduction are both transport processes. Viscosity can be described as a measure of the resistance of a fluid to flow. Liquid slags fall into the general class of Newtonian fluids. The viscosity of the slag has an important effect on the speed and the efficiency of the extraction and refining processes. At a constant composition, the mass transport and thermal transfer by diffusion and convection are

inversely related to the viscosity of the molten slag. As an example, the viscous slag may entrap the bubbles of gas emerging from the molten metal and form a foaming slag which is not desirable and results in increased slag volume. This requires an enlarged refining vessel to contain it and reduces the heat transfer rate significantly. Therefore, the viscosity of a slag must be low because the diffusion processes in the slag must occur quickly enough for the reactions between slag and alloy to approach equilibrium rapidly. This also affects the kinetics of the process favourably. When the furnace is tapped, due to the turbulence, small metal droplets entrapped in the slag and the rate at which these metal droplets are separated from the slag phase is a function of the slag viscosity. On the other hand, an excessively viscous slag gives rise to operational difficulties during tapping.

The viscosity is directly related to the ionic size or the molecular species present in the melt. Therefore, the viscosity of a liquid slag increases with an increase in the structural complexity. Thus, an increase in the concentration of basic oxides results in a decrease in the viscosity of the molten slag due to the silica network breaking up into smaller silicate anionic groups. An increase in the silica concentration as an acidic component shows the opposite effect and results in higher slag viscosities for all compositions more acidic than the metasilicate ratio. In the more basic compositions than the orthosilicate ratio, the discrete anions exist, therefore, the viscosity is not effected by structural considerations.

Liquidus temperature of slags is an important parameter in the operation of the process because, by using the liquidus temperature data, it is possible to determine the extent of slag overheating and therefore to obtain better heat utilisation. Liquidus temperature is also considered as a parameter to make estimations about slag viscosities and electrical conductivities

Number of investigators[42,43] studied the viscosities in the slags related to the ferromanganese production. Trekalo[42] found that an increase in MnO content decreases the viscosity and the liquidus temperature. The other investigators[43] found that the viscosity decreases with increasing MnO content of the slag and that this effect is even greater in acidic slags than in more basic slags. On the other hand, Balon, Gartman and Levin[43] observed a slight decrease in the viscosity with increasing MnO content. Kurnushko[44] also found that increasing MnO content decreased the viscosity and all of these slags were liquid at 1500°C with the possible exception of the slag containing the lowest MnO content.

Chubinidze and Kekelidze[43] showed that viscosity of silicomanganese slags decreased with increasing basicity of the slag at 1500°C. They also found that an increase in MgO content decreased the viscosity remarkably. Kekelidze and Samarin[45] studied the viscosity of medium-carbon ferromanganese slags and found out that with increasing MnO-to-CaO ratio the liquidus temperature and viscosity decreased for all MgO contents. However the change in the viscosity values were remarkably high at low temperatures and very low at

high temperatures. The substitution of MgO for CaO reduced both the liquidus temperature and the viscosity values.

Jakovenko and Kondakov[46] investigated the influence of MgO on the viscosity of the slags encountered in ferromanganese production. They found out that by reducing the MnO content and increasing the MgO content, the conditions of superheating of the slag were improved which in turn the viscosity was lowered.

Tanabe, Oku and Honda[43] investigated the viscosity of $CaO-MnO-Al_2O_3-SiO_2$ slags and found a sharp decrease in the viscosity with increasing MnO content. However, above the basicity of 1.32 and an increase in MnO content up to 20 mass per cent increased the viscosity. On the other hand, at constant MnO contents, the viscosity decreased as the Al_2O_3 content increased to a certain point, thereafter increased with further additions of Al_2O_3.

Kozakevitch[43] measured the viscosities of five different slags containing 16 to 20 mass per cent MnO and showed that slags with alumina contents of as high as 29 mass per cent could have liquidus temperatures below 1400°C and low viscosities. He explained that at low silica levels, the basic oxides were essentially equivalent in their effect on slag structure, however, at higher silica levels, the different cations began to impose different effects on viscosity of the slag.

Warren[47] also determined the liquidus temperature of the $MnO-CaO-MgO-SiO_2-Al_2O_3$ slags related to ferromanganese production in conjunction with the MnO activity measurements and found that the liquidus temperatures for slags with 13 mass per cent MnO were lower than those belong to the quaternary system $CaO-MgO-SiO_2-Al_2O_3$.

Woollacott et al.[48] measured the viscosities in $MnO-CaO-MgO-SiO_2-Al_2O_3$ slags at 10 mole per cent Al_2O_3. He found that SiO_2 plays a major role on the magnitude of viscosity and MnO had the greatest effect in decreasing the viscosity. MgO was less effective in decreasing the viscosity.

Electrical conductivity can be taken as a measure of the ease of mass transport caused by a gradient of electrical potential across a material. The electrical conductivity of silicate melts is generally considered to be entirely cationic, although this may be influenced by the anionic constitution. The slag must posses suitable electrical conductivity to allow the flow of the electric current and to generate the heat required in submerged arc electric furnace processes. Molten slags are ionic conductors and an increase in the amount of the network modifying oxides results in an increase in the electrical conductivity of the slag due to an increase in the concentration of conducting basic cations and the decreasing size of the silicate anion network.

The literature on electrical conductivities are limited compared to those on viscosities related to

ferromanganese slags. The increasing use of electric arc furnaces in the production of ferromanganese motivated the investigations in this field and the work done on electrical conductivities were usually performed in conjunction with viscosity measurements.

Kurnushko[44] studied electrical conductivities in conjunction with viscosities for slags containing 10 mass per cent MgO, 5 mass per cent Al_2O_3 and MnO up to 15 mass per cent. He observed that increasing the MnO content decreased viscosity and increased the electrical conductivity only slightly. Kekelidze and Samarin[45] found that MgO had a stronger effect on electrical conductivities than was suggested by Kurnushko[44].

Tanabe et al.[43] and Shubinidze and Kekelidze[49] carried out extensive investigations on electrical conductivities of MnO containing slags with wide composition ranges. Tanabe et al.[43] first studied the influence of MnO content from 5 to 25 mass per cent when the CaO-to-SiO_2 ratio varied between 0.78 and 1.43. They found that electrical conductivity was increased with increasing amount of MnO. An increase in the basicity up to about 1.1 increased the conductivity but thereafter decreased it. This decrease conflicts with the ionic theory of the slags. He also found that the effect of Al_2O_3 was not significant.

Schubinidze and Kekelidze[49] studied the silicomanganese slags and found that basicity had only a slight effect on

electrical conductivities. MnO was the only component effecting the conductivity. A slight increase was also observed by increasing the MgO content.

In a recent study, Eric, Hejja and Stange[50] studied the liquidus temperatures and the electrical conductivities in synthetic $MnO-CaO-MgO-SiO_2-Al_2O_3$ slags representing the slags produced from the operation of ferromanganese electric furnaces. According to this study, the electrical conductivity of these slags increased with increasing basicity ratio between the basicity values of 0.55 tc 1.1. The electrical conductivity was found to decrease depending on the MnO content at basicity ratios above 1.1. The liquidus temperatures were found to vary from 1300° to 1380°C. Increase in the basicity ratio increased the liquidus temperature. The electrical conductivity was found not to be effected significantly with the CaO-to-MgO ratios.

The surface tension is an important physical property for the wetting of metals and refractories by slags and for the rate at which various components dissolve in the slag. The surface tension information can be used for the calculation of interfacial tension and adhesion between metal and slag. The surface tension of liquid slags in general decreases with increasing silica content of the slag and decreases with the addition of alkali oxides, boric acid, calcium sulphide and phosphoric oxide, whereas lime, iron oxide and alumina increase the surface tension of the slag.

2.3.3 Thermodynamic properties of slags involving MnO

The distribution of manganese between the alloy and slag phases determines the overall recovery of manganese. This distribution is controlled by the thermodynamic characteristics of the furnace charge which consists of molten slag and metal phases; i.e., the equilibrium constants of reactions that take place and the activities of the components involved. The equilibrium constants are temperature dependent but the activities are less affected by temperature. At a particular temperature the equilibrium constant specifies the maximum recovery of manganese possible for given activity characteristics of reacting components. The activities may be described as the effective concentrations. Therefore, the recovery of manganese can only be improved by manipulating the compositions of slag and alloy phases such that the activity coefficient of manganese oxide in the slag should increase and the activity coefficient of manganese in the alloy should decrease. The reverse situation is desired in the case of elements if their contents in the alloy should be restricted. Normally only the slag composition is manipulated to achieve these, since metal composition is determined by standard specification. Thus, the thermodynamic activity information plays an important role in increasing the recovery of manganese in ferromanganese production.

Once optimum activity characteristics of the reacting components have been obtained, the next objective is to bring the reaction to equilibrium as close as and as quickly as possible. This would lead to the optimum recovery indicated by the thermodynamics of the process

and further would influence the rate of reduction as a possible production objective. The general agreement is that the manganese distribution is close to equilibrium in normal ferromanganese practise, whereas, the silicon distribution is not. The factors influencing the kinetics of the reduction reactions in a furnace producing high-carbon ferromanganese should be studied in order to determine the nature of the rate-limiting step of the reactions, as well as the extent of the positive effect of temperature increase[43].

The system $MnO-SiO_2$ was investigated by Glasser[51]. The conventional quenching technique was used and manganese was kept in the divalent state by working in an atmosphere of low oxygen partial pressure. The data gathered was used in constructing the equilibrium diagram of the binary system.

Abraham, Davies and Richardson[52] measured the activities of MnO at 1500°C and 1650°C in its melts with SiO_2, $CaO+SiO_2$, and $CaO+SiO_2+Al_2O_3$. The results indicated that MnO interacted with SiO_2 more strongly than FeO, but less strongly than CaO. For better recoveries, it was recommended that more basic slags are preferable to keep the MnO activities higher and SiO_2 activities lower. Their results are shown in Figures 9 and 10.

Mehta and Richardson[53] also measured the activities of MnO at 1500°C and 1650°C with SiO_2, $CaO+SiO_2$, $MgO+SiO_2$, $BaO+SiO_2$, $CaO+Al_2O_3$, and $CaO+SiO_2+Al_2O_3$. The amphoteric

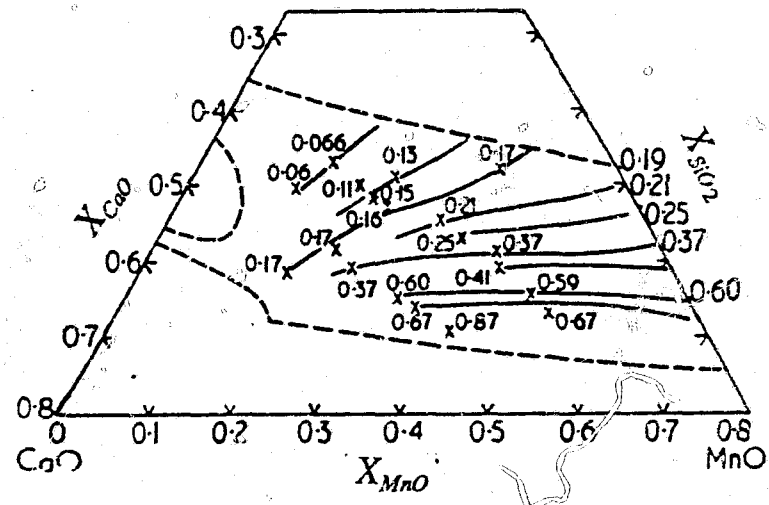


Figure 9. Activities of MnO in MnO-CaO-SiO_2 melts measured at 1500°C by Abraham et al.[52], dashed lines show the probable liquidus temperature in the system.

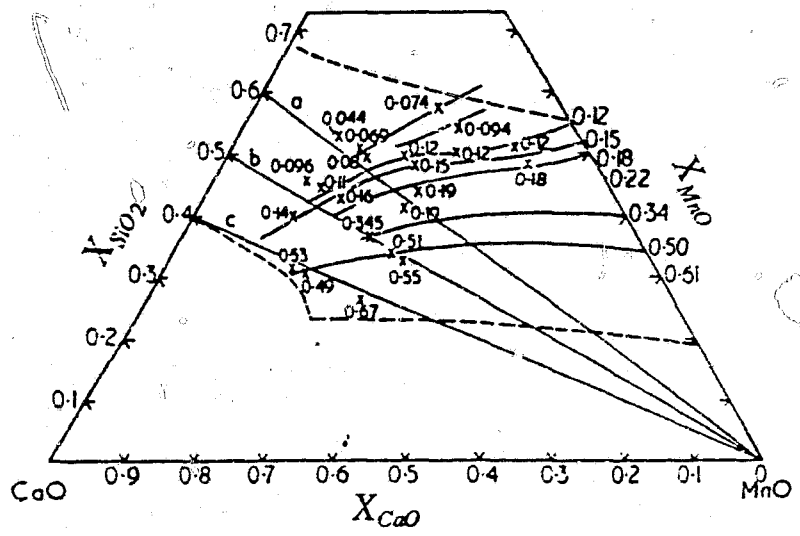


Figure 10. Activities of MnO in MnO-CaO-SiO_2 melts measured at 1650°C by Abraham et al.[52], dashed lines show the probable liquidus temperature in the system.

nature of alumina was well reflected in the activity coefficient pattern for MnO in $CaO+SiO_2+Al_2O_3$. Their results are shown in Figures 11, 12, 13 and 14.

Sharma and Richardson[54] measured the MnO activities at 1650°C in mixtures of $MnO+Al_2O_3$ and $MnO+SiO_2+Al_2O_3$. They also measured the sulphide capacities and derived the activity coefficient of the sulphides of manganese and magnesium. The activity coefficients of sulphides were greatest at compositions where the free energy of formation of the silicate mixtures had their maximum negative values. Their results are shown in Figures 15, 16.

In these works[52,53,54], manganese metal was dissolved into solid platinum which was in contact with manganese containing slag. The desired oxygen partial pressure was generated by mixing H_2, CO_2 and N_2. The activities of MnO in slags relative to the pure solid oxide were calculated by using the activity values of Mn in solid platinum[10]. The equilibrium exploited in these studies was given by:

$$(MnO) = [Mn] + \frac{1}{2}O_2 \quad \text{.....(17)}$$

The round brackets indicate components in the slag phase and square brackets indicate components in the metal phase.

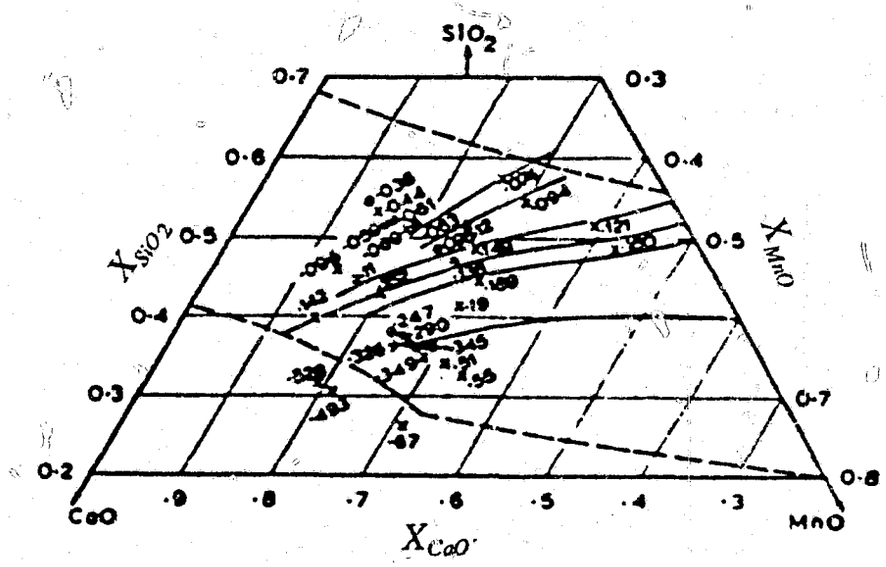


Figure 11. Activities of MnO in MnO-CaO-SiO_2 melts measured at 1650°C by Mehta and Richardson[53], dashed lines show the probable liquidus temperature in the system.

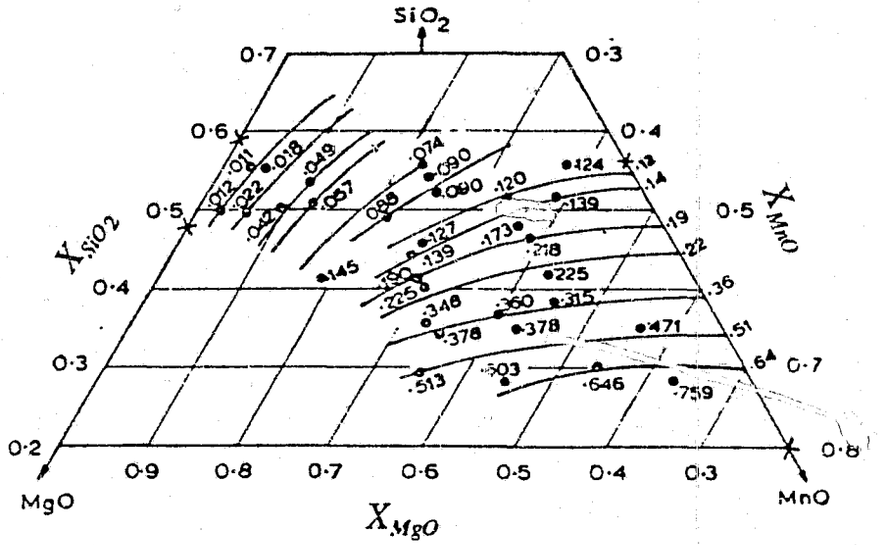


Figure 12. Activities of MnO in MnO-MgO-SiO_2 melts measured at 1650°C by Mehta and Richardson[53], crosses show liquidus limits in binaries.

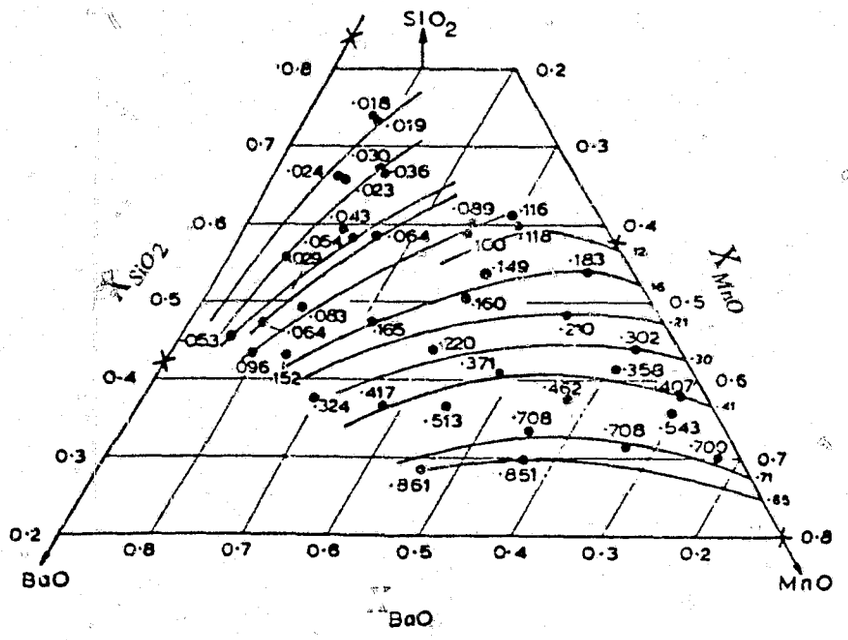


Figure 13. Activities of MnO in MnO-BaO-SiO_2 melts measured at 1650°C by Mehta and Richardson[53], crosses show liquidus limits in binaries.

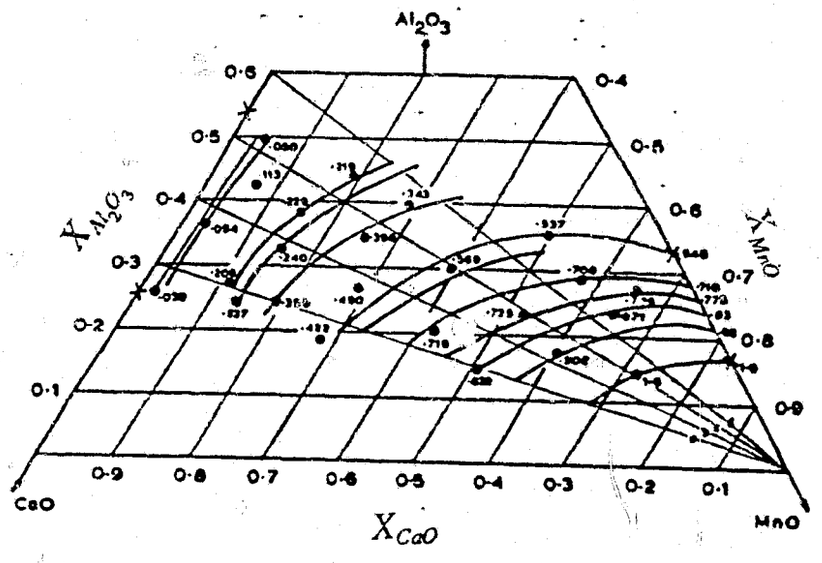


Figure 14. Activities of MnO in MnO-CaO-Al_2O_3 melts measured at 1650°C by Mehta and Richardson[53], the limiting activities in MnO-Al_2O_3 are taken from Sharma and Richardson[54], crosses show liquidus limits in binaries.

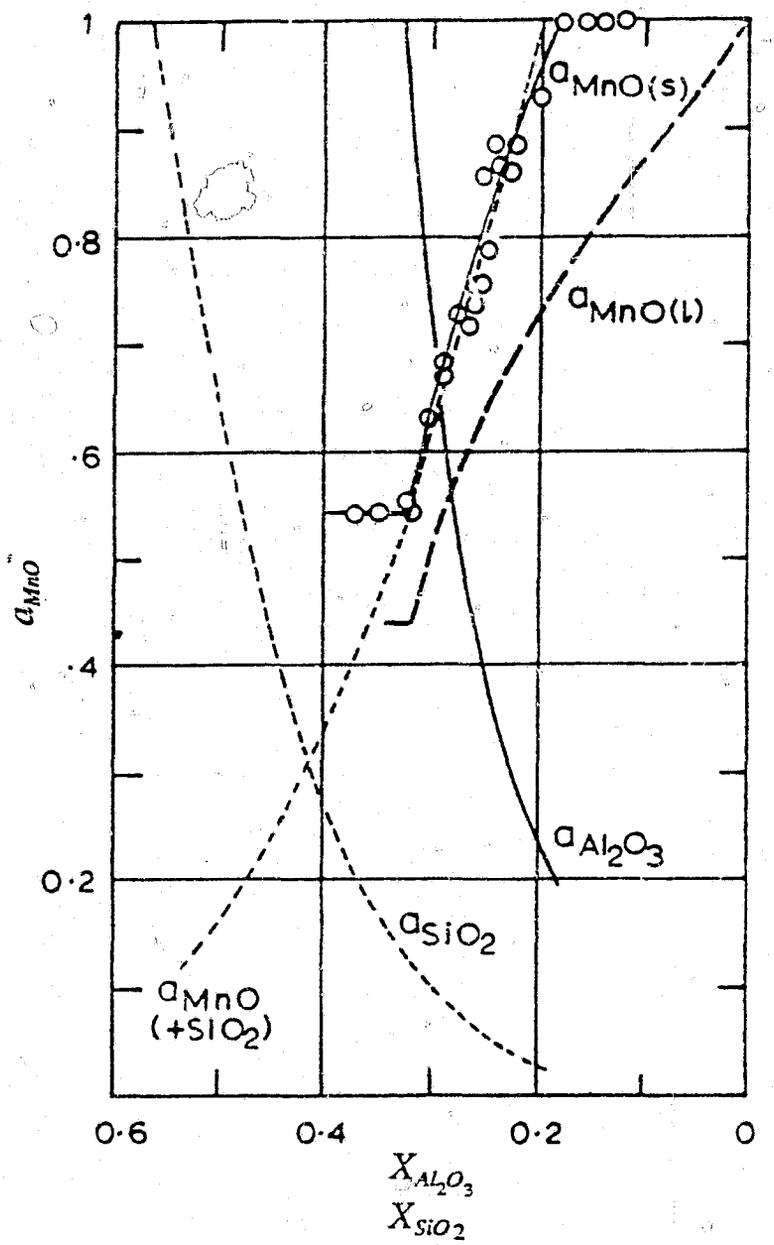


Figure 15. MnO and Al_2O_3 activities in MnO-Al_2O_3 melts measured at 1650°C by Sharma and Richardson[54]. Full lines and points represent results relative to solid MnO and Al_2O_3; heavy broken line relative to liquid MnO. Lightly broken lines show corresponding values for MnO and SiO_2 activities in MnO-SiO_2 melts at 1650°C taken from Abraham et al.[52].

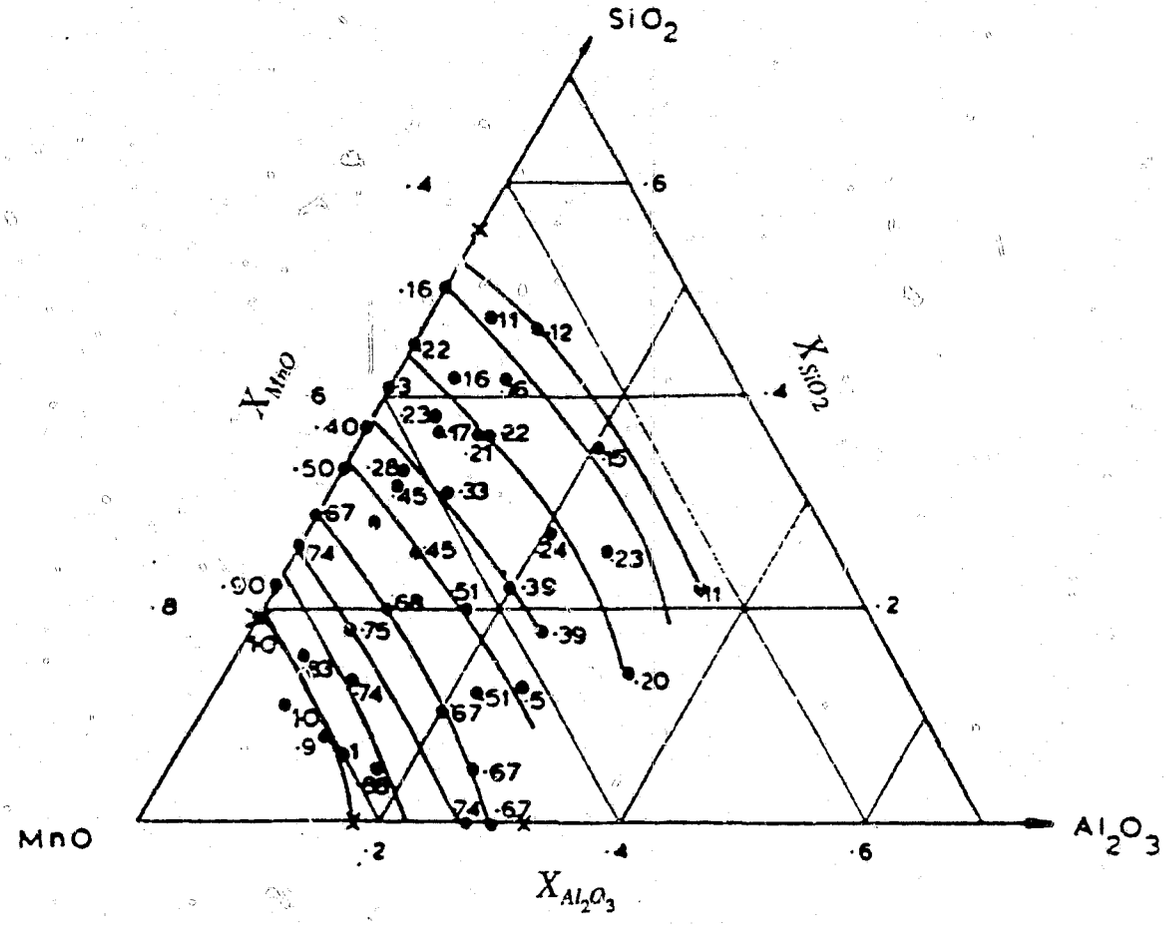


Figure 16. Activities of MnO measured at 1650°C by Sharma and Richardson[54] in $MnO-SiO_2-Al_2O_3$ melts relative to pure solid.

Filer and Darken[55] studied the equilibrium between blast furnace metal and slag phases in graphite crucibles. The effect of 5 mass per cent additions of individual slag components was studied in relation to the manganese distribution. They showed that MgO and CaO additions had basically the same effect of decreasing the (MnO)/[Mn] ratio but the silica increased this ratio while alumina had no effect. High basicity or temperature resulted in low (MnO)/[Mn] ratio, low temperature or high basicity favoured the low silicon content of metal. It was emphasized that the complete equilibrium was not achieved in the blast furnace which prevented the improvement of desulphurization and the manganese recovery.

Stukel and Cocubinsky[56] determined the distribution of manganese between metal and slag at 1450° and 1540°C. The equilibrium was described as:

$$(MnO) + C = [Mn] + CO \quad \text{.....(18)}$$

Graphite crucibles were used in the experiments. The slag samples contained 1-10 mass per cent MnO, 16-45 mass per cent CaO, 31-59 mass per cent SiO_2, 8-31 mass per cent Al_2O_3 and 0.1-0.8 mass per cent FeO. The MgO content was 5-11 mass per cent only for six experiments. They found that, for a given temperature, the manganese distribution approached equilibrium values, the distribution ratio (MnO)/[Mn] decreased as the CaO-to-SiO_2 ratio increased, and, for a given basicity, the recovery of manganese was enhanced by high

temperatures and low slag volumes. The range of manganese concentrations in pig iron did not affect the manganese distribution, alumina did not affect the recovery of manganese and up to 13 mass per cent substitution of MgO for CaO did not appear to affect the manganese distribution between metal and slag phases.

Turkdogan[57] made a further study of the data of Stukel and Cocubinsky[56] to calculate the activity of MnO relative to pure liquid MnO in these slags mentioned above. He derived the equilibrium constant of reaction (18) as

$$K = \frac{(a_{MnO})}{[a_{Mn}]} \quad \text{.....(19)}$$

since the activity of carbon would be 1 in a carbon saturated system and the CO atmosphere was considered to be 1 atmosphere. Then from the available data on the free energies of formation of MnO and CO from their elements in their standard states (pure liquid Mn and MnO, CO at 1 atmosphere and B-graphite), he obtained the free energy change of reaction (18) as:

$$\Delta G^0 = -225941 + 141.63T \quad (J/mole) \text{.....(20)}$$

and the temperature dependence of the equilibrium constant was given by

$$\log K = \frac{11890}{T} - 7.34 \quad \text{.....(21)}$$

where the K is as in equation (19). It was necessary to know the activity of manganese in carbon-saturated iron to evaluate the a_{MnO}. Due to the lack of data in activities of manganese in carbon saturated iron, he considered the thermodynamic properties of Fe-C melts. Since the similarity in the electronic configurations, it was permissible to assume that small percentages of Mn may not influence the activity coefficient of Fe and it was conceivable that the activity coefficient of Mn in these melts may not be very different from that of Fe. Therefore, he was able to predict the activity of manganese in carbon saturated Fe-Mn-C melts, and errors due to this estimation were not considered large enough to affect the subsequent activity calculations.

Turkdogan observed that MnO concentration did not effect its own activity coefficient. Therefore, the slag composition can be recalculated to give $CaO\%+SiO_2\%+Al_2O_3\% = 100$. Consequently, it was possible to draw iso-activity coefficient curves of MnO in the $CaO-SiO_2-Al_2O_3$ pseudo-ternary system. These curves are shown in Figure 17 within the range of composition in which Stukel and Cocubinsky worked[56], MnO activity was not affected by the temperature. Therefore, the iso-activity coefficient curves in Figure 17 were assumed to apply within a range of 1400°-1600°C.

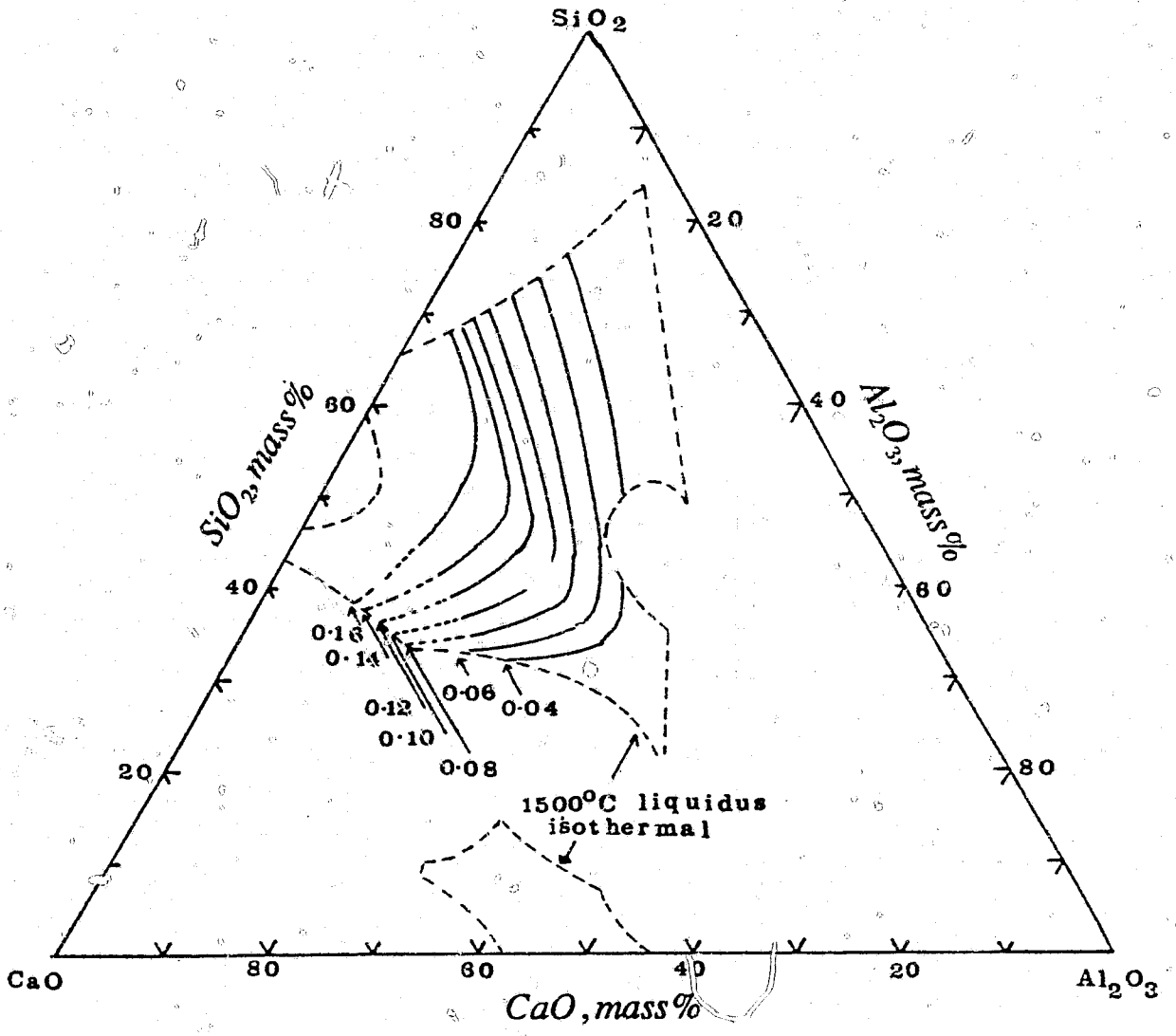


Figure 17. Iso-activity coefficient curves of MnO, calculated by Turkdogan[57] and drawn for $CaO-Al_2O_3-SiO_2$ pseudo-ternary system for the temperature range 1400°-1600°C; the liquidus isothermal drawn is for 1500°C.

The important features of the relationship in Figure 17 are as follows:

- For a given CaO content, the activity coefficient of MnO increases as Al_2O_3 is replaced by SiO_2,
- For a given SiO_2 content, activity coefficient of MnO increases as Al_2O_3 is replaced by CaO,
- For a given Al_2O_3 content, activity coefficient of MnO increases as SiO_2 is replaced by CaO at low CaO-to-SiO_2 ratios ($CaO:SiO_2=0.71$), but at higher basicities ($CaO:SiO_2=0.84$), further increase in CaO content of the slag, at the expense of SiO_2, decreases the activity coefficient of MnO.

The first two items were interpreted suggesting the existence of some bonding between the manganese cations and aluminate anions. In low basicities, replacement of SiO_2 by CaO, at a given Al_2O_3 concentration, is expected to weaken the binding forces between manganese and silicate ions, thus increasing the activity of MnO in the slag. However, he explains that an increase in CaO content for a given Al_2O_3 concentration will also reduce the interaction between aluminium and silicate ions so that, at higher CaO-to-SiO_2 ratios, aluminium cations would no longer be stable and would form aluminate anions which in turn would attract manganese cations, and consequently, the activity coefficient of MnO would become less.

Rankin[58] investigated the equilibrium between Mn-Si-C carbon saturated alloys and silicate slags that contained various amounts of CaO, MgO, and Al_2O_3. He adopted the approach, from a practical point of view, to

study the equilibrium by measuring the distribution ratios of Mn and Si or K′, the apparent equilibrium constant of reaction given by:

$$2(MnO) + [Si] = 2[Mn] + (SiO_2) \quad \text{.....(22)}$$

The variations with composition of a^2_{Mn}/a_{Si} in the alloys and a^2_{MnO}/a_{SiO_2} in the slags were obtained and the data was used to predict the equilibrium MnO contents of slags that were formed in the production of high-carbon ferromanganese and ferromanganese silicide. For a ferromanganese alloy of fixed composition, the equilibrium MnO content of the slag decreased with increasing additions of CaO, MgO, and Al_2O_3, the effect being greatest for CaO and least for Al_2O_3. He found a fairly good correlation between the equilibrium MnO content and the total amount of CaO, MgO, and Al_2O_3 in the slag, calculated as
$\Sigma MO = \%CaO + 0.8\%MgO + 0.5\%Al_2O_3$. ΣMO refers to the single composition parameter for a slag in equilibrium with an alloy for which the MnO content is unique. A small number of analysis of slag and metal from the production of ferromanganese were compared with values predicted from the equilibrium laboratory study and it was found that in the production of high-carbon ferromanganese and ferromanganese silicide the equilibrium of reaction (22) was not attained in practice.

In another study, Rankin[50] found a higher SiO_2 solubility than that of which Glasser[51] found in the MnO-SiO_2 system at 1450°C. The silica saturation level was found as 0.165 mole fraction. As it was expected from the equation (22), the equilibrium SiO_2 content of the slag was found to increase as the Si content of the alloy was increased. The recalculated activity values of MnO were changed only slightly by adopting the higher silica saturation limit whereas the activity of SiO_2 was significantly altered. The SiO_2 activities were calculated by Gibbs-Duhem equation.

Rao and Gaskell[60] measured the MnO activities in MnO-SiO_2 melts at 1400°, 1500° and 1600°C by the technique in which equilibrium was established between the melt, a gaseous atmosphere of fixed oxygen pressure and a Pt-Mn foil immersed in the melt. The activities of MnO obtained were significantly lower than those of the previous investigations[52,53], although a good agreement existed between the activity of MnO obtained at silica saturation and that measured by the previous investigators. A good agreement also existed between the corresponding solubilities of silica. The activities of SiO_2 were determined by Gibbs-Duhem equation. The integral molar free energies of formation of MnO-SiO_2 melts at 1400°, 1500°, and 1600°C and the partial molar heats and entropies of MnO and SiO_2 at 1500°C were calculated. The standard free energies of formation of $MnO.SiO_2$ and $2MnO.SiO_2$ were calculated from the activities of MnO and SiO_2 in the metasilicate and orthosilicate melts respectively. The composition of silica saturation (silica solubility) was found to be a significant function of oxygen pressure and hence Mn^{3+}/Mn^{2+} ratio in

the melt. The results obtained at 1500°C were compared with those of Abraham and his co-workers[52] and Mehta and Richardson[53] as it is seen in Figures 18 and 19. The activities of MnO obtained by Rao and Gaskell were significantly lower than those of the two previous investigations[52,53]. Although a very good agreement was found between the activity of MnO at silica saturation and that measured by Mehta and Richardson[53], good agreements also existed between the corresponding silica solubilities.

Rao and Gaskell[61] also studied the thermodynamic activities of MnO in the melts MnO-SiO_2, MnO-B_2O_3, and in pseudobinary sections in the MnO-TiO_2-SiO_2, MnO-TiO_2-B_2O_3 and MnO-SiO_2-B_2O_3 at temperatures in the range of 1400° to 1550°C with the same technique mentioned above. They observed that for a given mole fraction of MnO, the replacement of SiO_2 by TiO_2 increased the MnO activities, and the replacement of SiO_2 by B_2O_3 decreased the MnO activities which indicates that TiO_2 and B_2O_3 are, respectively, less acidic and more acidic than SiO_2. The differences in acidity also caused the solubility of MnO in the binary melts to increase starting from MnO-TiO_2, to MnO-SiO_2, and MnO-B_2O_3. The form of the variation of MnO activities, within the narrow composition range studied at 1400°C in the system MnO-B_2O_3, was characteristic of a system of polyions. The fluxing action of TiO_2 was explained qualitatively as being due to the Ca^{2+}-Ti^{4+} interaction decreasing the influence of the Ca^{2+}-O^- interaction. The fluxing action of B_2O_3 was explained in terms of B_2O_3 decreasing the activity of SiO_2 either by mutual depolymerization or by the formation of borosilicate anions.

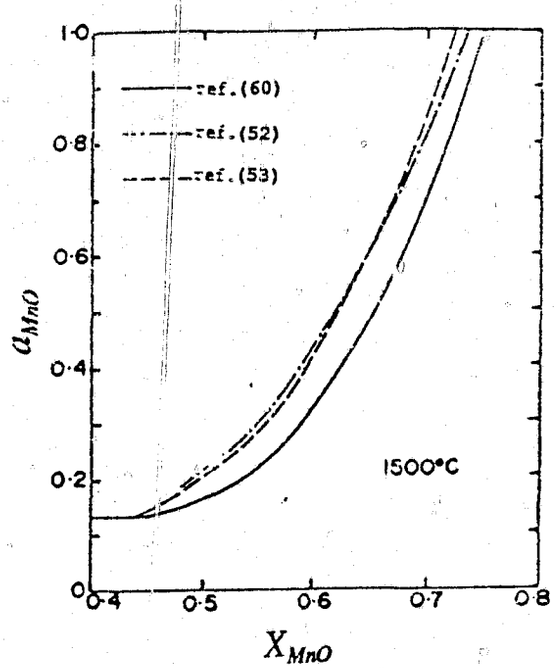


Figure 18. The activity of MnO in MnO-SiO_2 melts at 1500°C determined by Rao and Gaskell[60], Abraham et al.[52] and Mehta and Richardson[53].

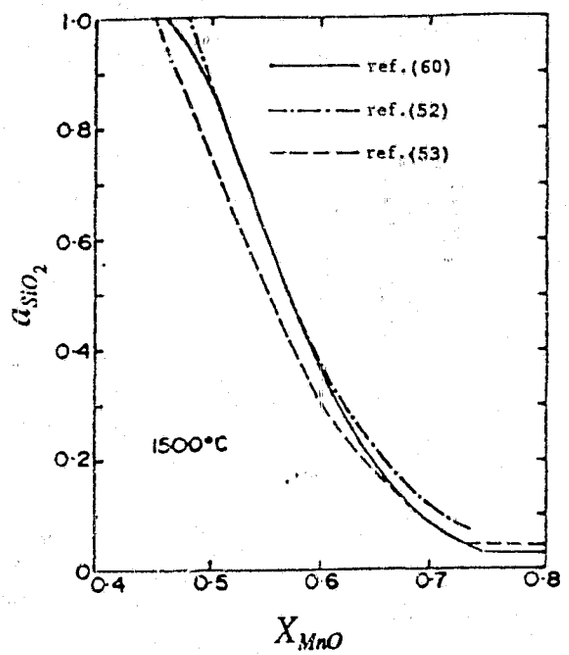


Figure 19. The activity of SiO_2 in MnO-SiO_2 melts at 1500°C determined by Rao and Gaskell[60], Abraham et al.[52] and Mehta and Richardson[53].

Turkdogan and Hancock[62] made an extensive study of Mn and Si distribution in systems of relevance to high-carbon ferromanganese production which was conducted at equilibrium under controlled laboratory conditions. The major findings of the study which pertain to the equilibrium of equation (22) are given as follows:

- For a given concentration of iron in the alloy, an increase in the CaO-to-SiO_2 ratio increases the silicon distribution ratio, but decreases the manganese distrib tion ratio,
- For a given CaO-to-SiO_2 ratio, the silicon distribution ratio increases with decreasing iron content of the alloy, whereas the opposite is true for the distribution ratio of manganese,
- In slags that contain Al_2O_3, the silicon and manganese distribution ratios increase as the Al_2O_3 content is reduced from 20 mass per cent to 0.

Toltstoguzov[63] found by a comparison of laboratory and plant data that the equilibrium of equation (22) was approached closely during the production of ferromanganese and ferromanganese silicide. The data were expressed in terms of K′, the apparent equilibrium constant of equation (22). For a constant silicon in the alloy, K′ was found to increase as the basicity of the slag was increased.

Selmer-Olsen[64] obtained slag and metal analyses from 52 taps of a 10-mVA submerged-arc furnace that produced high-carbon ferromanganese. The alloy had an approximately constant composition of 70-75 mass per cent Mn, 0.04-0.06 mass per cent Si and 6.8-6.9 mass per

cent C, but the MnO content and the basicity of the slag varied. In each case, the MnO content of slag was found to decrease as the basicity was increased. It was concluded that the most practical basicity formula for the plant operators to work with was the old-fashioned $\%CaO/\%SiO_2$.

Number of investigations have been done on the distribution of Mn between slag and metal relevant to iron and steelmaking. In these slags Mn is at low dilutions in molten iron. The equilibrium was described by:

$$(FeO) + [Mn] = (MnO) + Fe \quad \text{.....(23)}$$

[Fe] was omitted in the calculation of equilibrium constant since for dilute solutions of manganese in iron, a_{Fe} is approximately unity. The activity of a component in a phase is characteristic of the phase and not of the reaction used to obtain it nor of the multiphase system as a whole. Thus, when activities are used for the calculation of the equilibrium constant, a true equilibrium constant will be obtained and it will apply to all types of slags provided that the temperature and composition ranges of the slag are applicable to the process.

Korber and Oelsen[65] were among the first researchers who investigated the equilibrium with simple FeO-MnO and $FeO-MnO-SiO_2$, the latter mixtures having a composition

that ranged from 50 mass per cent MnO and 50 mass per cent SiO_2 to 48 mass per cent FeO and 52 mass per cent SiO_2. They described the equilibrium constant by:

$$\log K_{Mn} = \frac{7940}{T} - 3.172 \quad \text{.....(24)}$$

Chipman, Gero and Winkler[66] determined the temperature dependence of the value of the true equilibrium constant for the binary MnO-FeO system at 1550°C. They found that the activities of the oxides were equal to their mole fractions in the system. They expressed K_{Mn} by the following :

$$\log K_{Mn} = \frac{6440}{T} - 2.95 \quad \text{.....(25)}$$

It is found to be in good agreement with the calculated free energy change in the reaction, but was significantly higher than that obtained by Korber and Oelsen[65]. The slags used by Chipman and his co-workers[66] had a larger proportion of impurities which have a noticeable effect on the activities of the oxides.

Bell[67] studied the equilibrium between molten iron and slags containing FeO, MnO, MgO, and SiO_2 using both MgO and SiO_2 crucibles at 1550°C. The value of K_{Mn} was obtained as 3.5 which compared favourably with the value

obtained by Chipman and his co-workers[66]. The data obtained in this work on the distribution of manganese between metal and FeO-MnO-MgO-SiO_2 slags suggested that ideal mixing of silicates occurs in the system FeO-MnO-SiO_2 and FeO-MnO-MgO-SiO_2. Thus, it was possible to construct iso-activity curves for FeO, MnO, and SiO_2 in the system FeO-MnO-SiO_2 and to calculate the Mn, Si, and oxygen content of iron in equilibrium with these slags. Knowledge of this data is important in connection with deoxidation of steel by additions of manganese and silicon. The value of K_{Mn} which was found by Chipman and his co-workers[66] was also in good agreement with the results of Fischer and Fleischer[68] working with MnO saturated slags.

Bell, Murad and Carter[68] used the equilibrium constant of Chipman and his co-workers[68] and estimated the activities in the MnO-SiO_2 binary from their measurements with mixtures of MnO-FeO-SiO_2 slags at 1500°C. The slags were not saturated with silica and fell mainly between the orthosilicate join $2FeO.SiO_2$-$2MnO.SiO_2$ and the FeO-MnO side of ternary system FeO-MnO-SiO_2. They used a rotating crucible furnace and a wire-wound resistance furnace. The former appeared to give too high values for K_{Mn}. This was considered due to the effect of the continuous absorption of slag by the crucible used, or the sampling technique. Abraham, Davies and Richardson[52] criticised this approach as Bell and his co-workers assumed that the activity coefficient of FeO is unity in the ternary and that the activity coefficient of MnO depended only upon the mole fraction of silica in the binary and ternary systems. They added that this is not truly a valid assumption as one would expect the

activity coefficient of FeO to be raised by the presence of MnO and vice versa. Therefore, it would only strictly be possible to derive values for the ratio $a_{MnO} : a_{FeO}$. Richardson also pointed out that these authors failed to take into account the considerable amount of MgO dissolved into their slags from the magnesia crucibles used.

Turkdogan and Pearson[70] used the same equilibrium constant[66] to determine the a_{MnO} values in MnO-FeO-SiO_2 and some basic steelmaking slags. The activity of MnO in the slag was calculated from the equation given by:

$$a_{MnO} = K_{Mn} \ (a_{FeO}) \ Mn\% \qquad (26)$$

As mentioned above, K_{Mn} was calculated using the equation from Chipman and his co-workers[66] and a_{FeO} values were read from the ternary diagram[71]. When a slag composition was such that a_{FeO} values could not be derived from the iso-activity diagram[71] the activity was calculated from the oxygen content of the liquid iron in contact with the slag, and from the oxygen content of liquid iron in contact with pure iron oxide. They showed that the activity coefficient of MnO is independent of temperature within the range considered (1550° and 1650°C) and that the activity of MnO depends only on slag composition. They plotted a graph of a_{MnO} against concentration at 0.45, 0.47, 0.48, 0.52 and saturation silica mole fractions. In FeO-MnO-SiO_2 slags, rich in silica, MnO activity showed a negative deviation from

ideality, being greater than that found for FeO. This result was attributed to the greater stability of manganese silicates when compared with the ferrous silicates. In other words, MnO interacted with silica more strongly than FeO.

More complex steel making slags containing CaO, MgO, MnO, FeO, SiO_2 and P_2O_5 were divided into groups to investigate the effects of the influence of (CaO-MgO), (FeO) and (SiO_2-P_2O_5). This method was adopted due to the difficulties in investigating the effect of all the individual constituents. CaO and MgO; and SiO_2 and P_2O_5 were presupposed to have a similar influence on the molar basis on a_{MnO}. The slags were divided into groups of fixed ferrous oxide content (X_{FeO} = 0.05, 0.10, and 0.20) and MnO iso-activity diagrams were drawn for these three pseudo-ternary systems. It was shown that an increase in the proportion of (CaO+MgO), which means an increase in basicity, increased the a_{MnO} values. On the other hand, an increase in the FeO content decreased the a_{MnO} values in the slag.

Bishop, Grant and Chipman[72] equilibrated the liquid open-hearth type of slags with molten carbon-free iron in the temperature range 1530° and 1700°C. They used the equation (23) to calculate the activity of MnO in these slags and they plotted the iso-activity contours on the pseudo-ternary diagram
(CaO+MgO)-(SiO_2+Al_2O_3+P_2O_5)-(MnO+$(FeO)_T$). On a molar basis, they showed that an increase in the basicity ratio, given by (CaO+MgO)/(SiO_2+Al_2O_3+P_2O_5), to a value about 2.3 increased the value of the activity coefficient

of MnO. The activity coefficient of MnO then decreased as the basicity ratio increased above this value. A comparison of the influence of slag composition on the activity coefficients of MnO and FeO in the slags indicated that MnO is a more basic oxide than FeO, as generally accepted.

Jicheng et al.[73] measured the activities of MnO in blast furnace-type slags $CaO-SiO_2$, $CaO-SiO_2-Al_2O_3$ and $CaO-SiO_2-Al_2O_3-MgO$ at 1500°C in graphite crucible with Ag and Sn as solvent metals according to the reaction (18).

The agreement between the activity coefficients of MnO obtained from the experimental results using Ag and Sn separately as the solvent metal was good.

Warren[9] carried out the only study of the slags that are somewhat similar to those arising during the production of ferromanganese in South Africa. The slags consisted of MnO, CaO, MgO, SiO_2, and Al_2O_3 but the Al_2O_3 content was much higher than typical industrial slags. The liquidus temperatures and the activities of MnO at 1500°C were determined. The gas equilibration technique was used by the mixtures of H_2, CO_2 and N_2 gases. He found that the liquidus temperatures for slags with an MnO content of 13 mass per cent were lower than those belonged to the quaternary system $CaO-MgO-SiO_2-Al_2O_3$. The results can be summarized as follows:

-The liquidus temperatures of synthetic discard slags did not differ markedly from the liquidus temperatures recorded in the phase diagrams derived by Osborn et al.[74]

for the system $CaO-MgO-SiO_2-Al_2O_3$, being lower, on average, by about 30° to 40°C as mentioned before,
-The concentration of MnO in the slag did not affect its own activity coefficient within the compositional limits of the study,
-The substitution of some MgO for CaO in the more basic slags raised the activity coefficient of MnO. An increase in the Al_2O_3 content for given basicity ratio decreased the activity coefficient of MnO, especially in the more basic slags,
-The activities of MnO, the silica content of the slags, the liquidus temperatures, the viscosity data and the rate of reduction of MnO from the slags showed that the slags should be chosen

a. With as high a basicity ratio as possible
b. With some MgO, depending upon the Al_2O_3 content
c. With relatively high Al_2O_3
d. With low liquidus temperatures, and the liquidus isotherms widely spaced.

2.3.4 Slag Models

Slags have a very important role in most pyrometallurgical operations. In spite of this major role, precise information about their properties and behaviours is incomplete. Furthermore, when the experimental difficulties are concerned in determining their thermodynamic properties, the crude estimations obtained by using slag models are rather considered as reliable information. The most successful estimations such as the ones developed by Flood-Grjotheim's[75] model, although very important industrially, are limited to highly basic steelmaking slags. Elliot and his co-workers[76] revised this application due to an error in

the use of free energy. Grjotheim and Brun[77] applied this model to the experimental results investigating phosphorus and manganese distribution between slag and molten metal.

The most fundamental structurally-based slag models have been developed by Toop and Samis[78,79] and Masson[80]. Toop and Samis developed a theoretical treatment which allowed the most probable number of anions in any acid or basic silicate slag to be calculated in terms of an equilibrium constant for the equilibrium between singly bonded oxygen, O^-, doubly bonded oxygen, O^0, and free oxygen, O^{2-}, ions in the melt as described by equation (16):

$$O^0 + O^{2-} = 2O^- \quad \text{.....(16)}$$

In this approach, for binary silicate systems, the equilibrium constant was assumed to be characteristic of the cation.

Masson[80-82] expressed the distribution of anions in terms of ionic fraction rather than concentration of reactive groupings. Although this allows more specific conclusions to be reached regarding the concentration of polyionic species, the treatment is limited to melts of $X_{SiO_2} < 0.5$. In Masson's approach, two cases were considered: one in which the SiO_4^{4-} ion is considered to be a bifunctional mer unit and the other in which the SiO_4^{4-}

ion is considered to be a tetra functional mer unit. In the former case, only two of the $Si-O^-$ groups on any SiO_4^{4-} ion can react to form polysilicate ions and, therefore, only linear chain ion formation is possible and in the latter case four of the $Si-O^-$ groups on a SiO_4^{4-} ion may react, thus permitting the formation of branching chain ions. By making use of the vast experience in the studies of polymerization processes, Masson made some assumptions in his model:

-The intramolecular condensation may be neglected,

-All functional groups of the same kind are chemically equivalent,

-Ion fractions are related to thermodynamic activities by the Temkin equation

$$a_{MO} = N_{M^{2+}} \; N_{O^{2-}} \quad \text{.....(27)}$$

The first assumption implies that the silicate ions consist exclusively of linear and branched chains of general formula $Si_xO_{3x+1}^{2(x+1)-}$. The distribution of anions in such a system is considered in terms of the equilibrium constant for the reaction between the SiO_4^{4-} and any species of chain length x to yield the next higher member and free oxygen ion. Thus the depolimerization reaction can be written as:

$$SiO_4^{4-} + Si_xO_{3x+1}^{2(x+1)-} = Si_{x+1}O_{3x+4}^{2(x+2)-} + O^{2-} \quad \text{.....(28)}$$

When the constitution of binary silicate melts is considered in terms of linear chains alone, the equilibrium ratios, K_{1x}, for the reaction (28) are assumed to be independent of x. The chain growth by addition of monomer can occur at only two sides, namely, the ends of the chain, in linear chains. Similarly, depolimerization of monomer from the chain can also occur at two locations. Therefore the equilibrium constant for the reaction (28) is independent of chain length. Denoting the equilibrium constant for the reaction (28) to be K, the sum of the ion fractions of silicate anions is obtained as :

$$\Sigma N_{silicate} = N_{SiO_4} + N_{Si_2O_7} + N_{Si_3O_8} \quad \text{.....(29)}$$

Substituting for the individual ion fractions, the summation reduces to

$$\Sigma N_{Silicate} = \frac{N_{SiO_4}}{1 - \frac{KN_{SiO_4}}{N_{O^{2-}}}} \quad \text{.....(30)}$$

If silicate and oxygen are considered to be the sole ionic species in the melt,

$$\Sigma N_{Silicate} = 1 - N_{O^{2-}} \quad \text{.....(31)}$$

Substitution of which into equation (31) will give

$$N_{SiO_4} = \frac{1-N_{O^{2-}}}{1+K\frac{1}{(N_{O^{2-}}-1)}} \quad \text{.....(32)}$$

The mole fraction of silica in the binary melt was expressed in terms of N_{SiO_4} and $N_{O^{2-}}$, and using equation (32) and the Temkin's equation:

$$a_{MO} = N_{M^{2+}} \; N_{O^{2-}} \quad \text{.....(27)}$$

Masson derived the following expression:

$$\frac{1}{N_{SiO_4}} = \frac{3-K+a_{MO}}{1-a_{MO}} + \frac{K(K-1)}{\frac{a_{MO}}{(1-a_{MO})}+K} \quad \text{.....(33)}$$

The size distribution of silicate polyions was given by:

$$N_x = \left[\frac{1}{1+a_{MO}/K(1-a_{MO})}\right]^{x-1} \frac{1}{\frac{K}{a_{MO}}+\frac{1}{(1-a_{MO})}} \quad \text{.....(34)}$$

The value of K for various binary systems was obtained by curve fitting experimentally-determined

activity-composition relationships. In Figure 20 The calculated ionic distributions for $CaO-SiO_2$ and $FeO-SiO_2$ melts at 1600°C are shown.

Whiteway, Smith and Masson[83] derived the following theoretical equations for the size distribution of the polyions:

$$N_x = \frac{(3x!)}{(2x+1)!x!}\left(\frac{2\alpha}{3}\right)^{x-1}\left(1-\frac{2\alpha}{3}\right)^{2x+1}(1-N_{O^{2-}}) \quad \text{.....(35)}$$

N_x is the ion fraction of x-mer, α is the fraction of $Si-O^-$ groups present in the completely depolymerized state which have reacted to form doubly-bonded oxygen and free oxygen ions, and $N_{O^{2-}}$ is the ion fraction of free oxygen. From this distribution function and the Temkin equation, the activity of basic oxide expressed by a_{MO} was expressed in terms of mole fraction of SiO_2 and $K_{1,1}$ the equilibrium ratio for x=1, as:

$$\frac{1}{N_{SiO_2}} = \frac{1-\frac{1}{\frac{1}{3}+\frac{a_{MO}}{K_{1,1}(1-a_{MO})}}}{1-a_{MO}} + 2 \quad \text{.....(36)}$$

and the size distributions were obtained by:

$$N_x = \frac{(3x)!}{(2x+1)!x!}\left[\frac{1}{1+\frac{3a_{MO}}{K_{1,1}(1-a_{MO})}}\right]^{x-1}\left[\frac{1}{1+\frac{K_{1,1}(1-a_{MO})}{3a_{MO}}}\right]^{2x+1}(1-a_{MO}) \quad \text{.....(37)}$$

Ionic distributions were plotted for the system $FeO-SiO_2$ in the temperature range 1530°-1680°K and the value of $K_{1,1}$ was found to be 0.70. By curve-fitting the experimental activity-composition data to equation (36), the values calculated were inserted into the equation (37). Thus, the ion fractions of various species up to a decamer, $Si_{10}O_{31}^{22-}$ were calculated and shown in Figure 21.

The distributions closely resemble those calculated previously using linear chain model. Masson, Sommerville and Sosinsky[84] also extended the polymer theory to ternary silicate melts. They calculated the optical basicities of mixtures in the two ternary system which are $FeO-CaO-SiO_2$ and $FeO-MnO-SiO_2$ and the values of $K_{1,1}$ by interpolation

From the correlation between log $K_{1,1}$ and the optical basicities of these ternary systems found previously[38]. The calculated values of $K_{1,1}$ were used to calculate the ion fractions in the two ternary systems for compositions more basic than metasilicate.

Another approach using oxygen and cation sub-lattices was introduced by Yokokawa and Niwa[85]. A similar model to this was developed by Kapoor and Frohberg[86].

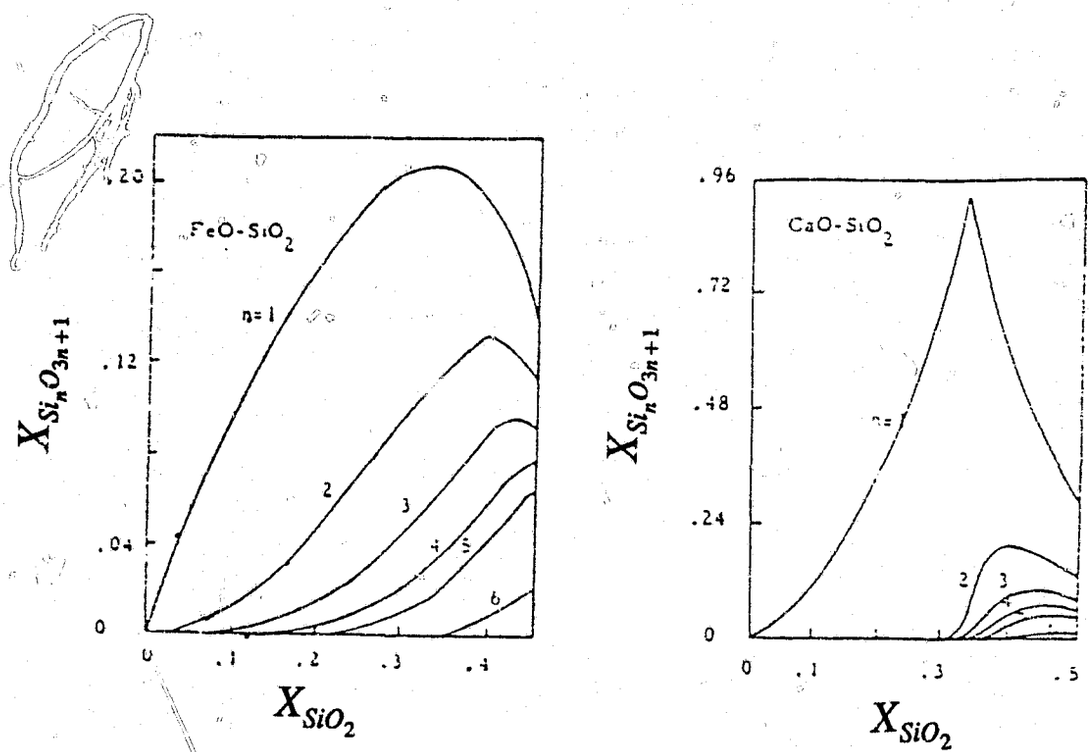


Figure 20. Ionic distributions for $FeO-SiO_2$ and $CaO-SiO_2$ melts at 1600°C calculated from Massons's[82] linear chain model.

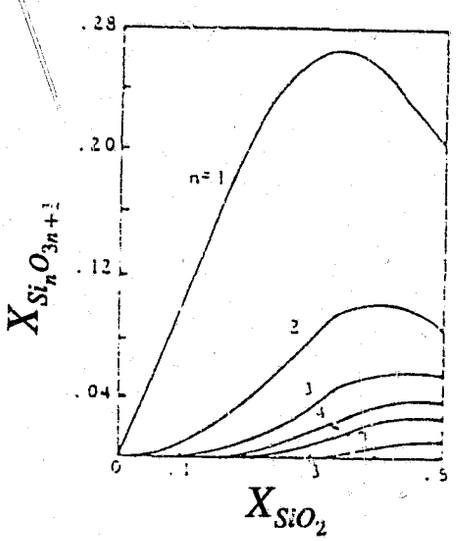


Figure 21. Ionic distributions for $FeO-SiO_2$ melts in the temperature range 1257°-1407°C calculated from the branched chain model developed by Whiteway, Smith and Masson[83].

According to this model, the properties of multicomponent systems are represented by using binary parameters.

Gaskell[87] has reviewed all these models and outlined the basics of the approaches used. In Gaskell's review, additional to the models already mentioned above, another structural slag model also outlined was of Lin and Pelton's[88]. According to this study , a structural model is given for binary silicate systems having $MO-SiO_2$ type where MO is a basic oxide and silicate tetrahedra and oxygen bonds are considered as structural units. The model considers the dependence of the enthalpy of the bonds on composition. One major advantage of this model is that it permits to calculate the numbers of ions of any configuration as it is not restricted to consideration of chain silicate ions.

A statistical model has been developed for complex slag systems by Gaye and Welfringer[59] and studies related to the same model have been carried out by Gaye and his co-workers[90-92]. The model of Kapoor and Frohberg[86] was extended to represent the properties of multicomponent systems. This statistical slag model was used to fit the results of the present work by making use of the equilibrium slag compositions. Therefore, the model will be explained in detail and discussed in section 4.1.2.

2.4 Thermodynamic properties of liquid manganese alloys

A number of authors determined the activities of components in liquid manganese alloy melts. Ohtani[93] measured the solubility of carbon in Fe-C-Mn melts at 1530±10°C up to about 40 mass per cent of manganese and obtained the following equation:

$$\Delta N_C^{Mn} = N_C^{Mn} - N_C^0 = 0.10N_{Mn} \quad \text{.....(38)}$$

where ΔN_C^{Mn} is the difference between solubility of carbon in Fe-C represented by N_C^0 and Fe-C-Mn represented by N_C^{Mn} being represented by mole fraction. The activities of manganese and carbon were determined at 1540°C in the range of Mn=0-40 and C=0-saturation mass per cent. He found[93] that the solubility of carbon increased gradually with increasing manganese content and the activities of manganese and carbon decreased gradually with the addition of carbon and manganese respectively. It was shown that interaction parameters play an important role in giving information on the behaviours of the alloying elements.

Schenk and Neuman[94] (1450°-1500°C), Petrushevskii and Gel'd[95] (1460°C) also found the same relationship between ΔN_C^{Mn} and N_{Mn}. Feldman[96] (1500°, 1600° and 1700°C) and Matoba and Banya[93] found the relationship as :

$$\Delta N_C^{Mn} = 0.11 N_{Mn} \quad \text{.....(39)}$$

Turkdogan and Leake[98] used the results of Chipman et al.[98] and showed that the difference ΔN_C^{Mn}; between carbon saturation in Mn-Fe-C ternary alloys N_C^{Mn} and that in iron-carbon binary melts N_C^0 is:

$$\Delta N_C^{Mn} = 0.1 N_{Mn} \quad \text{.....(40)}$$

Petrushevskii and Gel'd[95] determined the solubility of carbon in liquid Fe-Mn-Si-C melts at 1460°C. Their extrapolated results for the Mn-Si binary agree well with the results of Chipman et al.[99]. However, their results are somewhat lower than those of Turkdogan, Hancock and Herlitz[100]. These discrepancies between the results are small and are within the permissible experimental error. In Figure 22, the solubility of carbon in Fe-Mn-Si-C melts found[95] in this study is shown.

Burylev[101] calculated the carbon solubility in Mn-Fe-C (1290°, 1460° and 1490°C), Mn-Si-C (1400°C) and Mn-Fe-Si-C (1400° and 1460°C) systems in connection with the data obtained by number of authors[62,95,98,100]. He applied the regular solution model to these systems and the agreement between the calculated and experimental data was satisfactory up to 15 mass per cent Si in the melts. He also determined the energies of mixing for these systems more precisely. The solubility of carbon in Mn-Fe-Si-C system at 1400°C is shown in Figure 23.

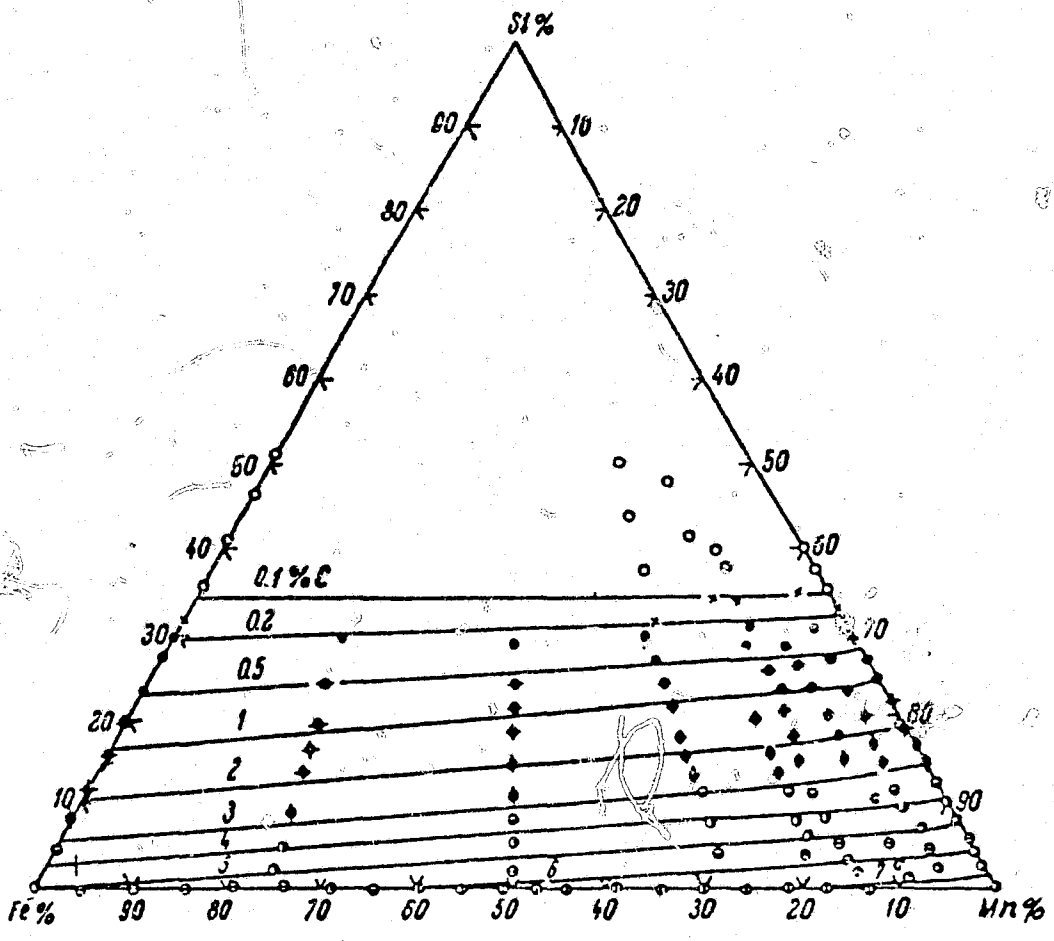


Figure 22. Solubility of carbon in Fe-Mn-Si alloys at 1460°C after Petrushevskii and Gel'd[93] on the assumption that Fe%+Mn%+Si%=100, the different points correspond to variations of carbon content from 0.10 to 7.5 mass per cent.

Esin and Vatolin[102] found lower solubilities of carbon than those determined by Petrushevskii and Gel'd[95] at 1460°C and expressed the carbon solubility in Mn-Si-C melts by:

$$\log N_C^{Mn,Si} = 0.56 - 0.8N_{Si} - 4.5N_{Si}^2 \quad \text{.....(41)}$$

Skiredj and Elliot[103] interpolated the results of Chipman et al.[99] who measured the solubility of carbon in Fe-Mn-C melts at 1290°, 1490° and 1690°C and drew the carbon solubility against the manganese content at 1400°, 1550°, 1600° and 1650°C shown in Figures 24 and 25. The results were in good agreement with those of Turkdogan et al.[104] and with Herty and Royer[105] except the discrepancies at low Mn-to-Fe ratios and in the binary system. Skiredj and Elliot[103] also used their own data and the interpolated data of Turkdogan and Hancock[62] and Herty and Royer[105] in the construction of carbon iso-solubility curves for the system Fe-Mn-Si-C at 1400°, 1550°, 1600° and 1650°C shown in Figures 26,27,28 and 29.

Yakushevich et al.[106] measured the solubility of carbon in silicomanganese melts between 1350° and 1800°C. They expressed the solubility of carbon in melts with up to 32 mass per cent silicon by the following equation where "C" is the solubility of carbon in mass per cent.

$$C = C_0 - 0.387Si^{0.95} + (1515 - 0.56T) \times 10^{-8}Si^{3.81} \quad \text{.....(42)}$$

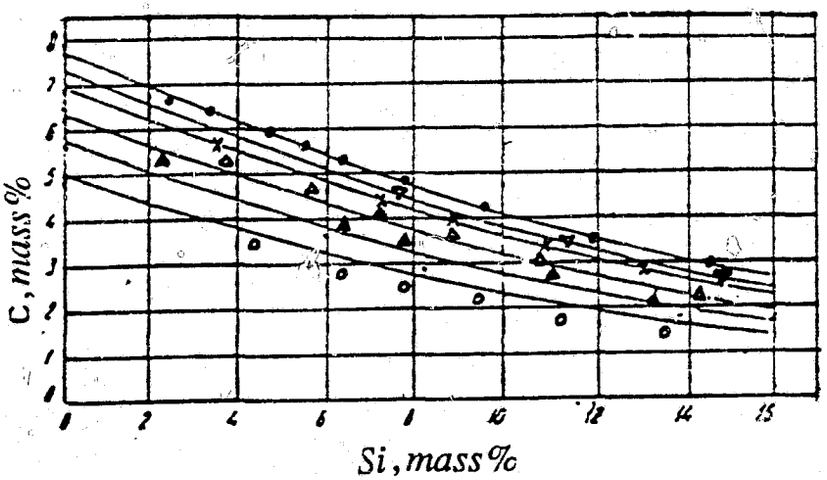


Figure 23. Solubility of carbon in the system Mn-Fe-Si-C at 1460°C after Burylev[101], Fe-to-Mn ratio equal to: o 0 (system Mn-Si-C); ▲ 0.2; △ 0.4; × 1.0; ▽ 3.0; and ● ∞ (system Fe-Si-C). Solid lines are calculated results.

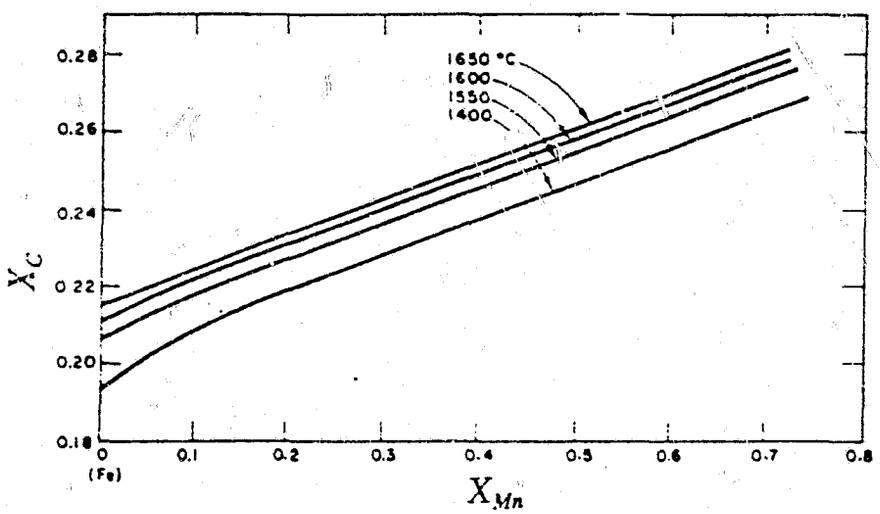


Figure 24. Solubility of graphite in Fe-Mn alloys reproduced from Skiredj and Elliot[103] using the data of Chipman et al.

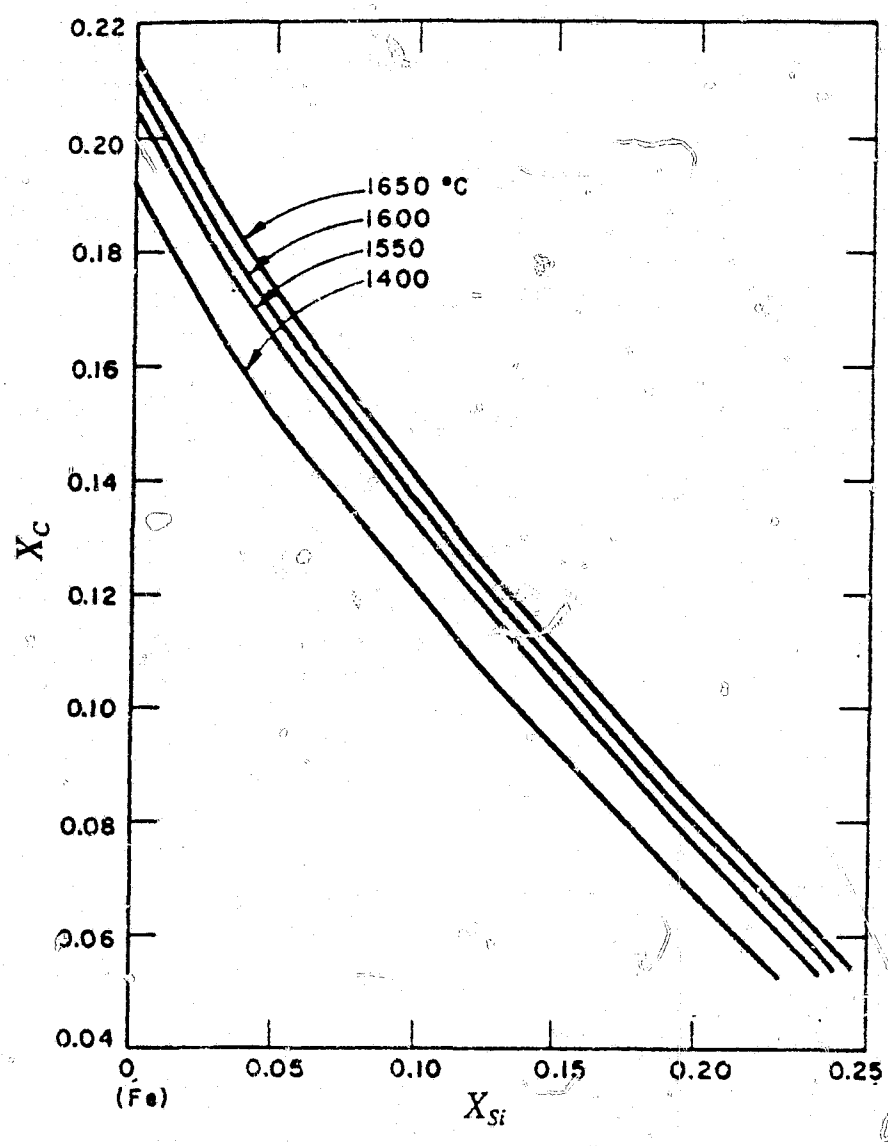


Figure 25. Solubility of graphite in Fe-Si alloys reproduced from Skiredj and Elliot[103] using the data of Chipman et al.

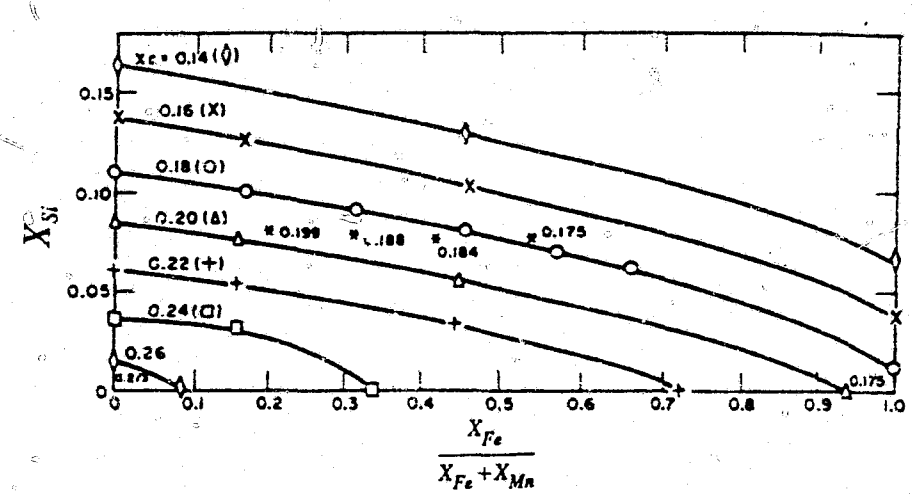


Figure 26. Solubility of graphite in Fe-Mn-Si alloys at 1400°C reproduced from Skiredj and Elliot[103] using the data of Turkdogan and Hancock and Herty and Royer.

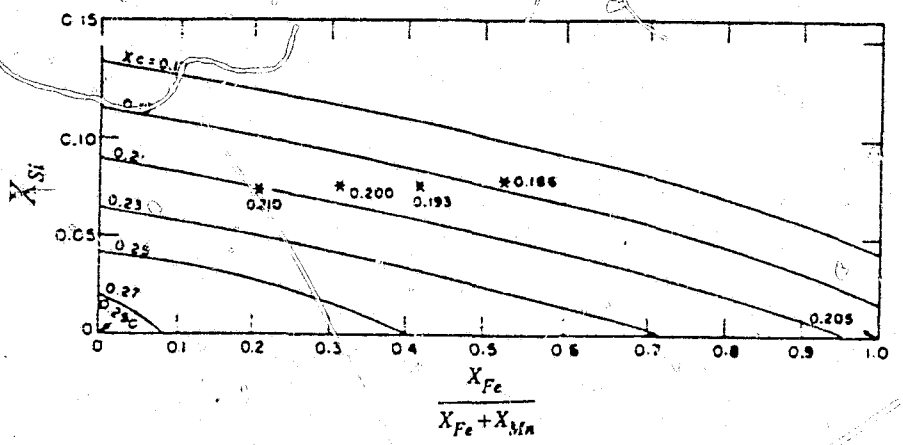


Figure 27. Solubility of graphite in Fe-Mn-Si alloys at 1550°C reproduced from Skiredj and Elliot[103] using the data of Herty and Royer.

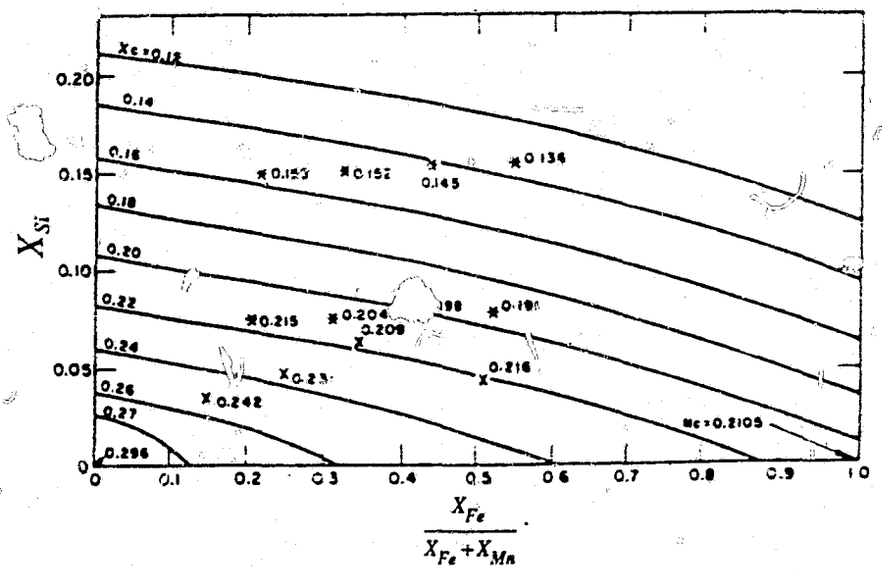


Figure 28. Solubility of graphite in Fe-Mn-Si alloys at 1600°C (× from Skiredj, * from Herty and Royer)[103].

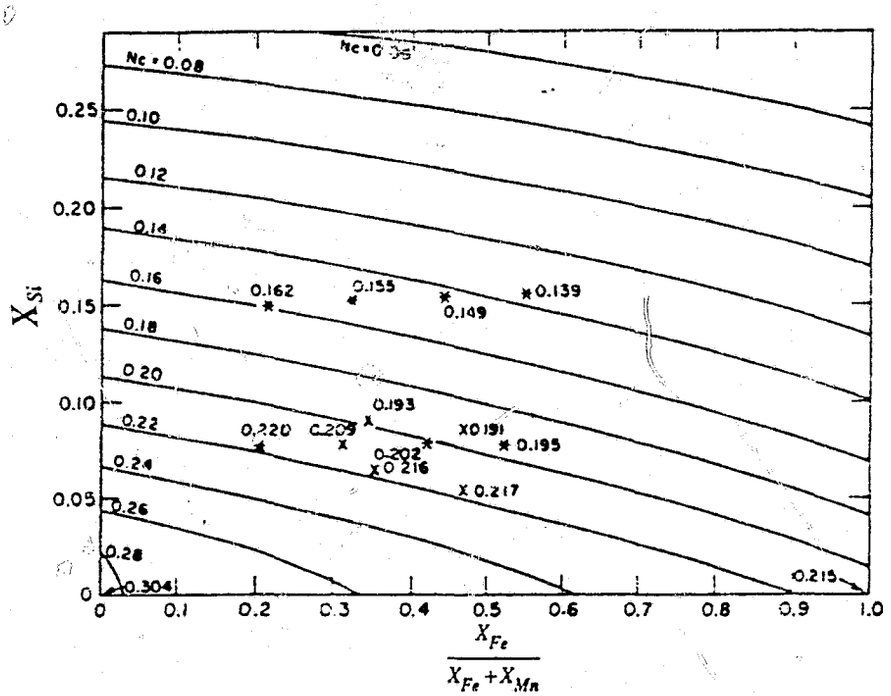


Figure 29. Solubility of graphite in Fe-Mn-Si alloys at 1650°C (× from Skiredj, * from Herty and Royer)[103].

In this equation, C_o is the mass percentage of carbon at zero silicon and was given by:

$$C_0 = 0.415 \times 10^{-2}T + 0.56 \quad \text{.....(43)}$$

The values calculated from equation (42) and (43) are somewhat different from the values given by Turkdogan[98].

Schultz, Riazance and Payne[107] determined the activities of manganese in Fe-Mn alloys at 1538°C by measuring the vapour pressure of manganese in equilibrium with the melts using the carrier gas method. It was found that Fe-Mn system was ideal. The results were in good agreement with those of Sanbongi and Ohtani[108] and Vatolin and his co-workers[109]. The latter authors used electrochemical methods to determine the activities.

Feldman[110] determined the activity of carbon and manganese in Fe-Mn-C alloys (up to 35 mass per cent manganese) at 1550°, 1600° and 1650°C. Ohtani[93] also measured the carbon and manganese activities at 1540°C in Fe-Mn-C alloys using an electrode concentration cell. The results of both authors were in good agreement. Ohtani obtained an empirical formula for the activity of manganese as:

$$a_{Mn} = N_{Mn} e^{-2.3 \times 3N_{Mn}N_C / (1-N_C)^2} \quad \text{.....(44)}$$

Wang and Chou[111], Vatolin et al.[109] and Schenk and Neuman[94] also measured the activity of manganese in Fe-Mn-C melts between 1460° and 1600°C. Their results were in good agreement with that of Ohtani[93] and Feldman[110].

Wada et al.[112] studied the effects of manganese and silicon on the activity of carbon in austenitic Fe-Mn-C and Fe-Si-C alloys by equilibration with controlled CH_4-H_2 atmospheres in the range of 848° to 1147°C and for composition up to about 60 mass per cent Mn and 7 mass per cent Si. They found that the activity coefficient of carbon was lowered by manganese and the effect of manganese on the carbon activity was proportional to the Mn content. Silicon increased the activity coefficient of carbon and the increase was a function of both the silicon and carbon contents.

Gee and Rosenqvist[113] used a transportation method to measure manganese vapour pressures over pure liquid manganese at 1244° and 1545°C and nine liquid Mn-Si alloys. In binary system, the derived manganese activities at 1527°C and the corresponding silicon activities calculated from the Gibbs-Duhem equation showed large negative deviations from ideality. In carbon saturated Mn-C melts, the manganese activities showed negative deviation from ideality in the range N_c=0-0.028 and the activity of manganese, at a fixed molar concentration, increased as silicon was replaced by carbon. At a fixed alloy composition, an increase in the temperature resulted in an increase in the manganese activity. For carbon saturated alloys, the activities of

manganese at 1527°C were lower than at 1427°C. This was explained with regards to the increased carbon solubility in the melts.

Tanaka[114] determined the manganese activities in Mn-C, Mn-Si melts by the vapour pressure measurements at 1400°C. The activities of manganese in Mn-C melts showed a positive deviation from ideality at less than 0.17 mole fraction of carbon. At higher mole fractions, a negative deviation was observed. The silicon activities in Mn-Si melts were calculated by the measured manganese activities in these melts and the Gibbs-Duhem equation. Remarkable negative deviations from ideality were observed.

Ahmad and Pratt[115] used a torsion-effusion technique to carry out vapour pressure measurements on twenty two Mn-Si alloys at temperatures between 1127° to 1627°C. The activities of manganese and silicon at 1427°C showed very strong negative deviations from ideality. The manganese activities computed from the vapour pressure data of Gee and Rosenqvist[113] and the data from Ahmad and Pratt[115] are in good agreement over most of the composition range except the deviations at the highest manganese contents. Excess free energies were calculated from the measured vapour pressures and were used to calculate the excess entropies of mixing in combination with the calorimetrically measured heats of formation. The excess entropies of mixing were found to be moderately negative.

Kor[116] determined the activity of silicon in Mn-Si melts at 1500°C. The equilibrium between Mn-Si melts and slags containing MnO, SiO_2, CaO and MgO were studied at 1400° and 1500°C in silica and magnesia crucibles. An empirical equation to predict the manganese and silicon distribution was obtained as function of the slag basicity at 1400° and 1500°C. A higher slag basicity and a lower activity of silica in the slag was obtained by the additions of up to 10 mass per cent CaF_2. This resulted in lower silicon contents in the metal phase. The presence of up to 20 mass per cent iron in Mn-Fe-Si melts decreased the activity coefficient of silicon. The effect of 1 to 2 mass per cent carbon in the metal on the equilibrium was roughly estimated and found to be almost negligible.

Tanaka[117] determined the activities of manganese in Mn-Fe-C, Mn-Si-C and Mn-Fe-Si-C melts by the same technique as in his previous work[114] at 1400°C. The results were shown by iso-activity curves. In the measurements, the atomic fractions of Fe, Si and C in Mn-Fe-C and Mn-Si-C melts were limited to lower than 0.25, the atomic fraction of Fe in Mn-Fe-Si-C melts to about 0.05 and 0.10 only, and the atomic fractions of Si and C to lower than 0.25. The iso-activity curves of Mn in the Mn-Fe-Si-C melts saturated with carbon at 1400°C are shown in Figure 30 a.

Dresler[118] evaluated the activities of carbon and manganese in the ternary system Fe-Mn-C for the temperature range 1400°-1800°C. The activities of carbon were determined by the Lupis and Elliot dilute solution

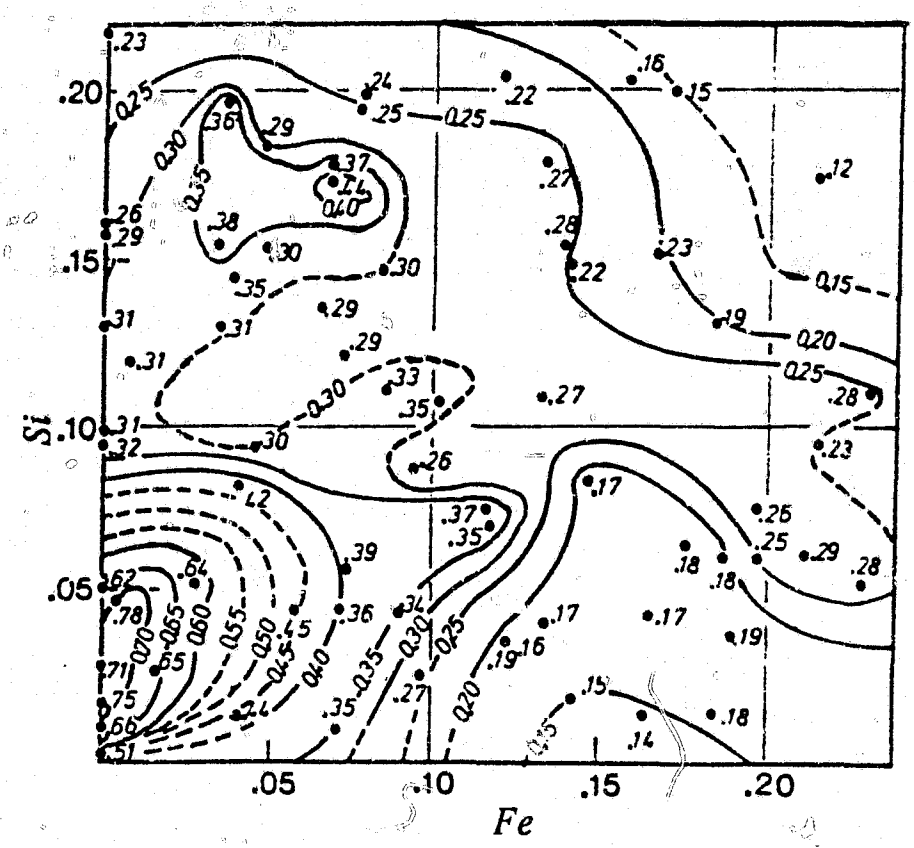


Figure 30 a. Isoactivity curves of Mn in the Mn-Fe-Si-C melts saturated with C at 1400°C[117].

approach. Manganese activities were calculated with Gibbs-Schumann integration for ternary systems. He found that carbon reduces manganese activity significantly, particularly at high carbon contents.

Tanaka[119] equilibrated the carbon saturated Mn-Si-C and Mn-Fe-Si-C alloy melts with $MnO-SiO_2$, $CaO-MnO-SiO_2$, $CaO-MnO-Al_2O_3-SiO_2$ and $CaO-MnO-Al_2O_3-MgO-SiO_2$ slags. From the experimental results, he calculated the following thermochemical values by making use of the activities obtained previously by himself and various investigators:

-The activities of Si in carbon saturated Mn-Si-C melts at 1500° and 1550°C, and in carbon saturated Mn-Fe-Si-C melts at 1500°C (Figure 30 b),

-The activities of SiO_2 in $CaO-MnO-SiO_2$ molten slags at 1500°C.

-The values of a^2_{MnO}/a_{SiO_2} in $CaO-MnO-Al_2O_3-SiO_2$ molten slags at 1500°C,

-The values of a^2_{MnO}/a_{SiO_2} in $CaO-MnO-Al_2O_3-MgO-SiO_2$ molten slags equilibrated with carbon saturated Mn-Fe-Si-C alloy melts at 1600°C (Figure 30 c).

Ni, Ma and Wei[120] determined the solubility of carbon in Mn-C, Mn-Fe-C, and Mn-Si-C melts at 1400° and 1500°C. The interaction coefficients e_C^{Si}, e_C^{Fe}, e_C^C were calculated.

Although it appears that a substantial amount of information has been available on manganese containing liquid alloy systems, the majority of these are related to conditions in iron and/or steelmaking where manganese

Author Cengizler H
Name of thesis Thermodynamic activity of Mn0 in Manganese slags and slag-metal equilibria 1993

PUBLISHER:
University of the Witwatersrand, Johannesburg
©2013

LEGAL NOTICES:

Copyright Notice: All materials on the University of the Witwatersrand, Johannesburg Library website are protected by South African copyright law and may not be distributed, transmitted, displayed, or otherwise published in any format, without the prior written permission of the copyright owner.

Disclaimer and Terms of Use: Provided that you maintain all copyright and other notices contained therein, you may download material (one machine readable copy and one print copy per page) for your personal and/or educational non-commercial use only.

The University of the Witwatersrand, Johannesburg, is not responsible for any errors or omissions and excludes any and all liability for any errors in or omissions from the information on the Library website.